

# Analyst

Accepted Manuscript



This is an *Accepted Manuscript*, which has been through the Royal Society of Chemistry peer review process and has been accepted for publication.

*Accepted Manuscripts* are published online shortly after acceptance, before technical editing, formatting and proof reading. Using this free service, authors can make their results available to the community, in citable form, before we publish the edited article. We will replace this *Accepted Manuscript* with the edited and formatted *Advance Article* as soon as it is available.

You can find more information about *Accepted Manuscripts* in the [Information for Authors](#).

Please note that technical editing may introduce minor changes to the text and/or graphics, which may alter content. The journal's standard [Terms & Conditions](#) and the [Ethical guidelines](#) still apply. In no event shall the Royal Society of Chemistry be held responsible for any errors or omissions in this *Accepted Manuscript* or any consequences arising from the use of any information it contains.

1  
2  
3  
4  
5  
6  
7  
8  
9  
10  
11  
12  
13  
14  
15  
16  
17  
18  
19  
20  
21  
22  
23  
24  
25  
26  
27  
28  
29  
30  
31  
32  
33  
34  
35  
36  
37  
38  
39  
40  
41  
42  
43  
44  
45  
46  
47  
48  
49  
50  
51  
52  
53  
54  
55  
56  
57  
58  
59  
60

## Silver nanostructures in laser desorption/ionization mass spectrometry and mass spectrometry imaging

Justyna Sekuła<sup>1</sup>, Joanna Nizioł<sup>1</sup>, Wojciech Rode<sup>2</sup> and Tomasz Ruman<sup>1\*</sup>

<sup>1</sup>*Rzeszów University of Technology, Faculty of Chemistry, Bioorganic Chemistry Laboratory, 6 Powstańców Warszawy Ave., 35-959 Rzeszów, Poland.*

<sup>2</sup>*Nencki Institute of Experimental Biology, 3 Pasteur Street, 02-093 Warsaw, Poland*

\*Correspondence to: prof. T. Ruman, Rzeszów University of Technology, Faculty of Chemistry, Bioorganic Chemistry Laboratory, 6 Powstańców Warszawy Ave., 35-959 Rzeszów, Poland, E-mail: tomruman@prz.edu.pl

### Abstract

Silver nanoparticles have been successfully applied as matrix replacement for the laser desorption/ionization time-of-flight mass spectrometry (LDI-ToF-MS). Nanoparticles, producing spectra with highly reduced chemical background in low  $m/z$  region, are perfectly suited for low-molecular weight compound analysis and imaging. Silver nanoparticles (AgNPs) can efficiently absorb ultraviolet laser radiation, transfer energy to the analyte and promote analyte desorption, but also constitute a source of silver ions suitable for analyte cationisation. This review provides an overview of the literature on silver nanomaterials as non-conventional desorption and ionization promoters in LDI-MS and mass spectrometry imaging.

*Keywords: low molecular weight compounds; mass spectrometry; mass spectrometry imaging; matrix-assisted laser desorption/ionization; matrix-free; matrixless; nanoparticles; silver nanoparticles*

## Contents

### Introduction

#### AgNPs in analysis of ionic compounds

#### AgNPs in analysis of non-ionic compounds

#### Silver nanostructures for microbial analysis

#### Active surfaces with silver nanostructures for LDI MS

#### AgNPs in LDI MS imaging

### Conclusions

### References

## Introduction

The number of studies utilizing the matrix-assisted laser desorption/ionization mass spectrometry (MALDI-MS) has significantly increased over the last 20 years. The MALDI-MS technique features excellent sensitivity and speed of analysis of ionic compounds, such as proteins, peptides, nucleic acids but also some non-ionic classes of chemical compounds such as lipids, etc.<sup>1-6</sup> Enabling detection within wide mass range, it is widely used in various fields of chemistry and biology.

Serious drawback in application of MALDI MS is the presence of matrix ions, causing suppression of analyte peaks.<sup>7-12</sup> The suppression effect can be avoided by application of matrixless methods, such as those based on various nanostructures. Nanostructures not only often allow reduction of spectral interferences in the low  $m/z$  range, but also greatly simplify the spectrum, as well as sample preparation. Moreover, nanostructure-based methods, especially those applying nanostructure-containing active surfaces, allow high degree of spot-to-spot reproducibility, thus avoiding the "sweet-spot problem."<sup>13</sup> A few years after

1  
2  
3 presentation of a MALDI methodology, based on organic matrices, Hillenkamp<sup>1</sup> and Tanaka<sup>14</sup>  
4  
5 experimented with mixtures of inorganic powders, testing their capacity to assist the  
6  
7 ionization. Tanaka was first to detect proteins and polymers using a two-phase system,  
8  
9 composed of ultrafine cobalt powders suspended in glycerol medium.<sup>15</sup> In 1995 Sunner et al.  
10  
11 applied inorganic particles, in the form of glycerol suspension, in place of organic matrices.<sup>16</sup>  
12  
13 Inorganic particles assist with the ionization process by absorbing laser energy and facilitating  
14  
15 thermal desorption of the analyte. Also other authors tested the use of nanometer- and  
16  
17 micrometer-sized metal particles suspended in glycerol and other liquids, the main  
18  
19 disadvantage of such approaches being severe “sweet spot” phenomenon, as well as problems  
20  
21 with vertical mounting of the sample holders.<sup>14,16-18</sup>  
22  
23  
24  
25  
26

27 Silver nanoparticles (AgNPs) in laser mass spectrometry usually act as an energy  
28  
29 receptacle for laser radiation. Laser energy dissociate the binding interaction between the  
30  
31 analyte and Ag particle surface, and transmit the analyte into the gas phase. AgNPs in  
32  
33 biomolecular analysis provides also additional advantages such as (i) have relatively high  
34  
35 tolerance of salts, (ii) elimination of interference of matrix-related ions, (iii) produce highly  
36  
37 reproducible signals, (iv) possibility of internal calibration due to silver-related ion peaks.  
38  
39 Moreover, antibacterial and antifungal activity of silver nanoparticles helps with preservation  
40  
41 of analyzed tissue.  
42  
43  
44

45 This paper is organized in five sections describing different aspects of the use of silver  
46  
47 nanomaterials in laser desorption/ionization mass spectrometry (LDI MS). First two chapters  
48  
49 covers the use of silver nanostructures in ‘conventional’ LDI MS analysis where silver  
50  
51 nanostructures are treated as ionization-facilitating additives of ionic and nonionic analytes.  
52  
53 Third chapter focuses on AgNPs in analysis of microorganisms and their fermentation  
54  
55 products, fourth on active surfaces containing surface-bound silver nanostructures. The fifth  
56  
57 chapter covers the application of silver nanostructures in LDI imaging of various surfaces.  
58  
59  
60

## AgNPs in analysis of ionic compounds

The mechanism of desorption and ionization on silver nanostructures is quite complex and not well understood. Usually, nanoparticles are believed to receive laser radiation and thermally-activated dissociation *via* rapid heating and explosive phase transition of analyte takes place. However, Silina et al. suggested that in case of palladium nanostructures there are an additional effects such as laser-induced acoustic desorption (LIAD) within the thin nanostructure layer, where ions are desorbed as a result of a mechanical ‘push’ rather than by heat. LIAD is triggered by acoustic pulses within thin layers, and varies strongly on the thickness of the layer.<sup>19</sup> Macdonald et al.<sup>20</sup> proposed a mechanism that anticipated the coordination of negatively charged stabilizing reagents to Ag nanoparticle shells, thus generating a negatively charged nanoparticle surface capable of capturing oppositely charged analytes through electrostatic interactions.<sup>21</sup>

Hua et al.<sup>21</sup> followed by others,<sup>22,23</sup> reported the nano-PALDI method with the use of citrate-stabilized AgNPs for an efficient desorption and ionization of a few peptides due to strong laser radiation absorption by nanostructures used and their high thermal conductivity.<sup>21-23</sup> Authors used two model peptides, bradykinin (0.1 mg/mL; Fig. 1A) and angiotensin I (0.5 mg/mL; Fig. 1B), in the presence of surfactants and salts, to examine potential of silver nanoparticles to act as matrix in ionization process.<sup>21</sup> Silver nanoparticles were synthesized by simple chemical reduction of silver nitrate by the earlier described method,<sup>24</sup> using 2 mM sodium cyanoborohydride in 1% sodium citrate solution to reduce rapidly stirred 5 mM silver nitrate. The resulting AgNPs were of  $160 \pm 20$  nm size and allowed adsorption of peptide analytes, as well as their desorption/ionization with little or no fragmentation.<sup>21,22</sup> The procedure described by Hua et al. recommended deposition on the

1  
2  
3 target plate of 0.5  $\mu\text{L}$  of the nanoparticle suspension, followed by 0.5  $\mu\text{L}$  of the analyte  
4  
5 solution and air drying.<sup>21</sup>  
6  
7  
8  
9

10 Please insert Fig. 1 here  
11  
12  
13  
14

15 In addition, Hua et al. showed silver nanoparticles to be suitable for  
16 desorption/ionization of peptides, with the resulting resolution of spectra obtained being  
17 identical to those of MALDI analyses using organic matrix. Moreover, in contrast to the  
18 authors' previous work formation of sodium/potassium adducts was not apparent.<sup>21</sup>  
19  
20  
21  
22  
23

24 Commonly known affinity of thiols to silver or gold ions was taken advantage of by  
25 Shrivastava et al.<sup>23</sup> to detect cysteine-containing peptides. The Authors successfully demonstrated  
26 that AgNPs can be employed as an efficient affinity probe in atmospheric pressure matrix-  
27 assisted laser desorption/ionization ion-trap mass spectrometry (AP-MALDI-ITMS) for  
28 analysis of biothiols such as glutathione or thiopeptides in urine. Bare AgNPs (10 and 20 nm),  
29 prepared by the reduction of silver ions with  $\text{NaBH}_4$  are capable of preconcentrating biothiols  
30 in the process of their determination in urine samples. This method was successful with the  
31 vacuum surface-assisted laser desorption/ionization (SALDI) MS but failed with AP-MALDI-  
32 MS, due to poor sensitivity of the latter.<sup>23</sup> Furthermore, the SALDI-MS analysis of sulfur  
33 drugs and biothiols was possible using bare, cetyl trimethylammonium bromide- (CTAB) and  
34 citrate-capped AgNPs, without the need of additional separation or washing. Proposed general  
35 structure of AgNP, its surface modified with analyzed biothiols, is presented on Fig. 2.<sup>23</sup>  
36  
37  
38  
39  
40  
41  
42  
43  
44  
45  
46  
47  
48  
49  
50  
51  
52  
53  
54

55 Please insert Fig. 2 here  
56  
57  
58  
59  
60

1  
2  
3 Bare NPs, compared to CTAB- and citrate-capped AgNPs, exhibited the best  
4 ionization efficiency. This effect being attributed to high affinity of bare AgNPs to biothiols  
5 due to formation of Ag–S covalent bonds. Adsorption of biothiols onto the surface of bare  
6 AgNPs resulted in 4–15-fold enhancement in sensitivity of analysis of the sulfur compounds  
7 studied.<sup>23</sup>

8  
9  
10 Considering the described interactions of noble metal nanoparticles with  
11 biomolecules,<sup>25-27</sup> Shrivastava et al.<sup>28</sup> applied for analysis of neutral peptides and proteins  
12 modified silver nanoparticles (AgNPs) with hydrophobic ligands, including dodecanethiol and  
13 octadecanethiol, prepared in toluene *via* liquid–liquid microextraction (LLME). The same  
14 group developed a single-step method of a single drop microextraction (SDME) for extraction  
15 of peptides from biological samples using silver nanoparticles. The silver nanoparticles were  
16 prepared by the reduction of AgNO<sub>3</sub> with NaBH<sub>4</sub> in aqueous system, followed by  
17 nanoparticle derivatization and transfer into organic phase, containing dodecanethiol or  
18 octadecanethiol. Modified AgNPs were usually smaller than 50 nm.<sup>28</sup> Besides, formation of  
19 tetraalkylammonium bromide-capped AgNPs was also described.<sup>29</sup>

20 Capped nanostructures prepared in toluene were used as electrostatic affinity probes to  
21 preconcentrate peptide mixtures from biological samples prior to AP MALDI ion trap mass  
22 spectrometer analysis. AgNPs coated with tetraoctylammonium bromide (TOAB) in toluene  
23 were prepared by reduction of AgNO<sub>3</sub> with NaBH<sub>4</sub> in two phase system containing TOAB in  
24 toluene. Analyzed peptides were injected into AgNP/toluene suspension, and, after a simple  
25 work-up, placed on to the target plate for MS analysis.<sup>29</sup>

26 In 2010 Kailasa et al.<sup>30</sup> reported the use of Ag<sub>2</sub>Se nanoparticles modified with  
27 octadecanethiol (ODT) and 11-mercaptoundecanoic acid (MUA) as extracting probes for  
28 analysis of hydrophobic peptides and proteins in aqueous solutions. The functionalized  
29 Ag<sub>2</sub>SeNPs were prepared in the reaction of silver nitrate, selenium powder and

1  
2  
3 octadecylamine, conducted at 180 °C for 10 min. NPs obtained as toluene suspension  
4 exhibited spherical shapes and the sizes were ranging from 7 to 10 nm. Analysis of peptides  
5 required mixing of toluene suspension of functionalized Ag<sub>2</sub>SeNPs (8.48 μmol) with peptide  
6 mixture (0.40 μM valinomycin and 0.80 μM gramicidin D) and vortexing for appropriate  
7 extraction time, followed by placement of 2 μL of organic phase with equal volume of CHCA  
8 matrix solution on the MALDI plate (Fig. 3).  
9  
10  
11  
12  
13  
14  
15  
16

17  
18  
19  
20 Please insert Fig. 3 here  
21  
22  
23

24 The Ag<sub>2</sub>Se/ODT NPs and Ag<sub>2</sub>Se/MUA nanoparticles served as good hydrophobic  
25 nanoprobe, allowing effective extraction of peptides in the presence of interfering  
26 substances, such as urea, Triton X-100 and sodium chloride.<sup>30</sup>  
27  
28

29 Shastri and co-workers presented recently preparation, characterization and examples of  
30 applications of silver nanoparticles modified with two different surface capping reagents that  
31 include 1-octadecanethiol/4-aminothiophenol and 1-octadecanethiol/1-thioglycerol pairs.  
32 Authors obtained interesting results for microextraction and identification of protein  
33 biomarkers and also tested their method with milk and urine as a 'real' samples. There was  
34 10–15 fold improvement in the signal intensity for 1-octadecanethiol/4-aminothiophenol-  
35 nanoparticle system observed compared to the conventional MALDI-ToF-MS.<sup>31</sup>  
36  
37  
38  
39  
40  
41  
42  
43  
44  
45  
46  
47

48 Recently Inuta et al.<sup>32</sup> presented analytical methodology, combining localized surface  
49 plasmon resonance (LSPR) sensing and matrix-assisted laser desorption/ionization-mass  
50 spectrometry using triangular silver nanoplates (AgNPLs) immobilized on solid substrates.  
51 The AgNPLs were prepared in a simple reaction system, utilizing silver nitrate, trisodium  
52 citrate and sodium borohydride. The first step of this synthesis was preparation of citrate-  
53 protected AgNPL seeds from spherical AgNPs by borohydride reduction of AgNO<sub>3</sub> in  
54  
55  
56  
57  
58  
59  
60

1  
2  
3 presence of trisodium citrate, followed by  $550\pm 100$  nm light irradiation at  $50^{\circ}\text{C}$ . The second  
4  
5 step of this synthesis was deposition of Ag on the AgNPL seeds to facilitate further lateral  
6  
7 growth of AgNPLs up to 30-70 nm size. Silver structures were then modified by attachment  
8  
9 of trypsin by *N*-(3-dimethylaminopropyl)-*N'*-ethylcarbodiimide hydrochloride/*N*-  
10  
11 (benzyloxycarbonyloxy)succinimide (EDC/Cbz-OSu) amine-carboxylic acid method. The  
12  
13 trypsin-modified AgNPLs were tested as soybean trypsin inhibitor (SBTI) probes after  
14  
15 immobilization of trypsin-AgNPLs on the MALDI plate with additional sinapic acid as a  
16  
17 matrix.<sup>32</sup>  
18  
19  
20  
21  
22  
23  
24

25 Please insert Fig. 4 here  
26  
27  
28

29 The resulting spectrum of the Trp/SBTI-AgNPL system shows molecular ions of SBTI at the  
30  
31  $m/z$  value of around 20100, indicating that the analyte could be desorbed and ionized during  
32  
33 the MALDI process (Fig. 4).<sup>32</sup>  
34  
35

36 Yang et al.<sup>33</sup> applied the zeolite immobilisation of 20-35 nm AgNPs, in order to  
37  
38 improve the stability of AgNPs. It was found that nanoparticle-zeolite system (AgNPs-  
39  
40  $\text{NH}_4\text{ZSM}_5$ ) could work as an efficient  $\text{Ag}^+$  donor. Authors anticipated zeolite to act as a heat  
41  
42 bath preventing AgNPs destruction after photoexcitation. The new material was applied for  
43  
44 LDI MS of ionic and nonionic biologically active substances of low molecular weights,  
45  
46 including acetylsalicylic acid, L-histidine, glucose, urea, cholesterol, and also small  
47  
48 compounds in human serum. Fig. 5 shows that compounds of interest in human serum were  
49  
50 observed as pairs of peaks of  $^{107}\text{Ag}^+$ - and  $^{109}\text{Ag}$ -adducts with relatively no peaks of sodium or  
51  
52 potassium-adducts.  
53  
54  
55  
56  
57  
58  
59  
60

Please insert Fig. 5 here

## AgNPs in analysis of non-ionic compounds

Sherrod et al.<sup>22</sup> used Ag-olefin interactions for selective ionization of sterols and lipids in the presence of commercial 20 nm and 60 nm silver colloids, without additional washing or extraction. They analyzed a sample, consisting of a mixture of 12 compounds of different polarity, using matrix mixture composed of DHB (2,5-dihydroxybenzoic acid) and silver nitrate (Fig. 6A) or only AgNPs (Fig. 6B). Of particular interest is the fact that only dehydrated cholesterol was observed as proton adduct with the use of organic matrix. At the same time, in the case of AgNPs-assisted ionization (Fig. 6A), peaks of intact cholesterol, indicating its presence as silver adducts, were found accompanied by relatively large  $\text{Ag}_2^+$  and  $\text{Ag}_3^+$  ion peaks (Fig. 6B).<sup>22</sup>

Please insert Fig. 6 here

Please insert Fig. 7 here

The same group successfully utilized 20 nm AgNPs to facilitate ionization of two carotenoids,  $\beta$ -carotene and phytoene, from a sample of carrot juice (Fig. 7), being a complex mixture of vitamins, minerals, terpenoids, lipids, carbohydrates, sugars, proteins, carotenoids and amino acids. Fig. 7 shows LDI spectrum in which only two signals correspond to a carotenoid and a carotenoid precursor, specifically  $[\beta\text{-carotene+Ag}]^+$  and  $[\text{phytoene+Ag}]^+$  at  $m/z$  643.3 and 651.4, respectively. It should be noted that both compounds reflected in the spectrum are of low-to-very low polarity.<sup>22</sup>

In 2008 Chiu et al.<sup>34</sup> applied silver nanoparticles as matrices for determination of three estrogens, E1, E2, and E3, with the use of surface-assisted laser desorption/ionization mass

1  
2  
3 spectrometry (SALDI-MS). Following preconcentration, compounds were adsorbed on the  
4  
5 AgNPs and directly analyzed with the detection limits for estrone (E1), estradiol (E2), and  
6  
7 (estriol) E3 found to be 2.23, 0.23, and 2.11  $\mu\text{M}$ , respectively. The silver nanostructures used,  
8  
9 34 $\pm$ 3 nm in diameter, were prepared by a slightly modified method of Lee et al.,<sup>35</sup> using  
10  
11 aqueous silver nitrate solution boiled with addition of trisodium citrate.  
12  
13  
14  
15  
16  
17

18 Please insert Fig. 8 here  
19  
20  
21  
22  
23  
24

25 Fig. 8 presents the mass spectrum resulting from simultaneous analysis of E1-E3  
26  
27 estrogens in negative ion mode in which ion peaks at  $m/z$  269.6, 271.5, and 287.5 were  
28  
29 assigned to the [E1-H]<sup>-</sup>, [E2-H]<sup>-</sup>, and [E3-H]<sup>-</sup> anions. The interactions between the AgNPs and  
30  
31 the three estrogens were confirmed as causing a shift in their surface plasmon resonance  
32  
33 (SPR) band from 410 to 436 nm.<sup>34</sup>  
34  
35

36 Wang et al.<sup>36</sup> analyzed aminoglycoside antibiotics in human plasma samples by  
37  
38 SALDI-MS using silver-coated AuNPs (Au/AgNPs). It is assumed that citrate-capped  
39  
40 Au/AgNPs attract positively charged aminoglycosides through electrostatic interactions.  
41  
42 Negatively charged silver nanoparticles were synthesized using a seed-mediated growth  
43  
44 method with trisodium citrate as capping compound. The bimetallic nanoparticle synthesis  
45  
46 involved mixing of AgNO<sub>3</sub> aqueous solution and colloidal gold solution, followed by addition  
47  
48 of this mixture into hydroquinone solution under stirring, yielding Au/AgNPs of mean  
49  
50 diameter of 39 $\pm$ 5 nm. Analytical method for bimetallic nanoparticles involved mixing the  
51  
52 Au/AgNPs suspension with aminoglycoside solution, shaking for 1 h and then centrifugation  
53  
54 for 10 min. After removal of the supernatant, nanoparticles were washed with water,  
55  
56 deposited on a target plate and air-dried. The detection limits of aminoglycosides in plasma  
57  
58  
59  
60

1  
2  
3 samples were found to be 9, 130, 81, and 180 nM for paromomycin, kanamycin A, neomycin,  
4  
5 and gentamicin, respectively.<sup>36</sup>  
6  
7

8 Gholipour et al.<sup>37</sup> were the first to examine the capabilities of NPs of diamond, silver,  
9  
10 titanium dioxide, barium strontium titanium oxide ((BaTiO<sub>3</sub>)(SrTiO<sub>3</sub>), BaSrTiO), and  
11  
12 titanium silicon oxide ((SiO<sub>2</sub>)(TiO<sub>2</sub>), TiSiO) for in situ MALDI-MS analysis of carbohydrates  
13  
14 from plant tissues. In their study, commercial silver nanoparticles smaller than 20 nm were  
15  
16 used for LDI of standard sucrose and fructans in positive and negative ion modes. Authors  
17  
18 state that All NPs studied, could also desorb/ionize carbohydrates from tissue in negative ion  
19  
20 mode. However, no signal was detected for AgNP system in positive ion mode. It must be  
21  
22 noted that this observation is rather unexpected for silver nanoparticles and might originate  
23  
24 from aggregation, too high concentration of stabilizing agents or too high pH value of AgNP  
25  
26 or AgNP-analyte suspensions.  
27  
28  
29  
30

31  
32 In 2012 Nie et al.<sup>38</sup> demonstrated the ability of commercial, 20 nm AgNPs to mediate  
33  
34 dual Surface-enhanced Raman spectroscopy and LDI MS (SERS/LDI-MS) detection,  
35  
36 acquiring information from solid phase samples without further sample preparation and  
37  
38 cleanup. It is believed that SERS enhances LDI-MS data by enabling extraction of chemical  
39  
40 information in the presence of matrix-related background. For LDI experiments, silver  
41  
42 nanoparticles in methanol-water system containing citrates was mixed with 1 mM analyte  
43  
44 citrate buffer solution and deposited on an indium tin oxide (ITO) conductive glass substrate.  
45  
46 The compounds that were chosen for analysis using this method, *p*-aminothiophenol,  
47  
48 rhodamine 6G and cholesterol, exhibit different strengths of interaction with AgNPs. Peaks of  
49  
50 *p*-aminothiophenol were found as clusters containing 1-3 silver ions/atoms and *p*-  
51  
52 aminothiophenol molecules in contrast to single peak of rhodamine 6G protonated adduct and  
53  
54 cholesterol silver adduct.<sup>38</sup>  
55  
56  
57  
58  
59  
60

1  
2  
3  
4  
5  
6  
7  
8  
9  
10  
11  
12  
13  
14  
15  
16  
17  
18  
19  
20  
21  
22  
23  
24  
25  
26  
27  
28  
29  
30  
31  
32  
33  
34  
35  
36  
37  
38  
39  
40  
41  
42  
43  
44  
45  
46  
47  
48  
49  
50  
51  
52  
53  
54  
55  
56  
57  
58  
59  
60

Preisler group has shown off-line SALDI analysis for LC-separated sterols such as cholesterol, 6-ketocholestanol,  $\beta$ -sitosterol, stigmasterol, campesterol and brassicasterol. Authors developed a methodology in which sample saponification followed by extraction of the unsaponifiable fraction with diethyl ether was followed by separation on a C18 column using methanol-water gradient. Samples for SALDI MS analysis were prepared using the automated sample spotting of colloidal suspension of silver over analyte layer. The SALDI MS LODs were found to be as low as 12 and 6 fmol for cholesterol and  $\beta$ -sitosterol respectively.<sup>39</sup>

Silver oxide nanostructures synthesized by wet precipitation method were found to be an cationisation agents acting similarly to silver nanostructures as shown by Taira et al. Authors investigated the nanoparticle assisted LDI process of thymine and hair growth promoters – *t*-flavanone and minoxidil that were found on spectra as proton-, sodium-, silver-107 and -109 adducts.<sup>40</sup>

### **Silver nanostructures for microbial analysis**

MALDI MS with silver nanostructures was used for characterization of species of pathogenic bacteria, with silver nanoparticles used as affinity probes to capture whole microorganism cells. AgNPs provide a high surface-to-volume ratio, resulting in high binding efficiency.<sup>41</sup> However, a sufficient number of bacterial cells, typically  $\sim 10^4$  cells per analysis, is required to generate MALDI-MS ion signals, therefore samples from infectious biological fluids or food poisoning samples are difficult to characterize directly by MALDI-MS.

A difficult problem in MALDI/nano-PALDI/SALDI analysis of microorganisms is connected with antibacterial and antifungal properties of silver and its nanostructures, a subject which is widely documented in the literature. The antimicrobial activity is more visible with increasing concentrations of AgNPs and results in decreased microbial protein

1  
2  
3 signals in mass spectrum. This problem was noticed not only for silver, but also for some  
4  
5 other nanoparticles such as TiO<sub>2</sub> and ZnO. Therefore controlling the nanoparticle  
6  
7 concentration in MALDI-MS bacterial analysis is a key factor.<sup>41</sup> This important subject of  
8  
9 MALDI/nano-PALDI/SALDI microbial analysis and identification with the use of  
10  
11 nanostructures was recently reviewed by Chiu.<sup>41</sup> Similar subject was also studied by Bright's  
12  
13 group who described MALDI mass spectrometry for generating marker profiles directly from  
14  
15 unfractionated microorganisms, such as viruses, bacteria, fungus cells and spores.<sup>42</sup> In parallel  
16  
17 Yao et al.<sup>43</sup> described the use of MALDI-MS for the identification and characterization of  
18  
19 peptides, as well as proteins, from “intact” micro-organisms.  
20  
21  
22  
23

24  
25 Unmodified silver nanoparticles were used as affinity probes for *Escherichia coli* and  
26  
27 *Serratia marcescens* by Gopal et al.,<sup>44</sup> to increase the sensitivity of MALDI-MS. Their  
28  
29 findings suggest that synthesized silver nanoparticles of 50-100 nm size must be used in  
30  
31 proper concentrations for affinity capture of bacteria from yogurt samples. The same research  
32  
33 group presented studies where AgNPs were added to bacteria during their early growth phase,  
34  
35 in order to allow microorganisms to adapt to the presence of foreign particles.<sup>45</sup> Furthermore,  
36  
37 they described the use of MALDI-MS in assessing the quality and shelf life and  
38  
39 microorganisms of yogurt.  
40  
41  
42

43  
44 Unmodified AgNPs were used as affinity probes to increase sensitivity of MALDI-MS  
45  
46 analysis for detecting in food samples common microbes, such as *E. coli*, *S. marcescens*, *B.*  
47  
48 *lactis*; *L. acidophilus*, *S. thermophilus*, *L. bulgaricus*, *L. acidophilus*, *B. longum*, *L. bulgaricus*  
49  
50 and *S. thermophilus*.<sup>44</sup> The interactions of bacteria with nanostructures which are responsible  
51  
52 for MALDI detection and identification of microbial compounds were also analyzed.<sup>46</sup>  
53  
54  
55  
56  
57  
58  
59  
60

## Active surfaces with silver nanostructures for LDI MS

MALDI has not been applied too often to detect low molecular weight (LMW) compounds, of MW < 600 Da, because common MALDI matrices are low molecular weight organic acids, producing a variety of matrix-related ions, causing interfering signals in the low-mass range.<sup>40,45,46</sup> This problem may be partially solved with surface-assisted laser desorption/ionization (SALDI) approach that was originally developed by Sunner et al.<sup>16</sup>. In SALDI desorption/ionization process is performed with help of active surface and no 'traditional' organic matrix is used. SALDI surfaces often contain organic, inorganic or metallic micro- or/and nanostructures. SALDI should be considered as a general term including nanostructure-dependent methods such as AuNPET, AgNPET, nanostructure-assisted laser desorption/ionization (NALDI),<sup>49</sup> nanoparticle-assisted desorption/ionization (nano-PALDI), or methods utilizing DIOS surfaces and others,<sup>50</sup> with strict condition that mentioned nanostructures were bound to target surface prior to sample application. It should be noted that besides the NALDI is a rather general term describing nanostructure-aided desorption/ionization, it is used mainly for target containing silicon nanowires on its surface produced by Bruker Daltonics company (Germany). Nanoparticle-based family of methods allows also soft ionization, without decomposition of the analytes, and analysis of a wide range of chemical compound classes.<sup>51</sup> SALDI methods utilizing AgNPs show great potential for effective absorption of laser energy to be transferred to the target molecules for desorption and ionization.<sup>52-54</sup>

Literature search proves that silver is a powerful cationisation agent, often used in mass spectrometry for various olefinic species, such as cholesterol and fatty acids, but also for medium and low polarity polymers. AgNPs have been also demonstrated to allow efficient capture of different chemical compounds (including amino acids, cholesterol, fatty acids) on their surface, thus efficiently promoting their desorption and gas-phase cationisation. The

1  
2  
3 minimum detectable amount for those organic and biological molecules is often in the fmol  
4  
5 range.<sup>23</sup> The use of silver nanoparticles in LDI-MS is presently raising a great deal of interest,  
6  
7 therefore in this review, LDI efficiency of methods based on silver-containing surfaces was  
8  
9 evaluated.  
10

11  
12 Wei et al. introduced an innovation of MS analysis of small molecules by  
13  
14 desorption/ionization on porous silicon (DIOS),<sup>55</sup> a variant of SALDI. It was the first LDI-MS  
15  
16 method utilizing electrochemically etched porous silicon surface, serving as absorber of UV  
17  
18 laser energy and allowing effective measurements of biomolecules in the absence of organic  
19  
20 matrix. This approach was further developed by application of several types of nanoparticles  
21  
22 (Ag, Au, P, HgTe, ZnS, nanocrystalline TiO<sub>2</sub>, MnO<sub>2</sub>, Mn<sub>2</sub>O<sub>3</sub>).<sup>56</sup> The main disadvantage of  
23  
24 porous materials is loss of SALDI activity after evaporation of water, a process that may take  
25  
26 place within few days.  
27  
28  
29  
30

31  
32 An improved, silver-based, DIOS method for LDI MS was proposed few year ago by  
33  
34 Xiao group. Porous silicon surface was modified by electroless plating of AgNPs *via*  
35  
36 reduction of Ag<sup>+</sup> ions by metastable hydrosilicon species. Compounds that were tested in this  
37  
38 work were tetrapyridinporphyrin (TPyP), oligomers of polyethylene glycol (PEG 400 and  
39  
40 2300), and a peptide of oxytocin. Authors showed LOD values for PEG400, PEG2300,  
41  
42 oxytocin and TPyP to be as low as 3.0 pmol, 30 pmol, 400 fmol and 5 fmol respectively.  
43  
44 However, it must be noted that porphyrins are known to have matrix-like properties and thus  
45  
46 aren't the best choice for testing compounds.<sup>57</sup>  
47  
48  
49

50  
51 Dufresne et al. explored the utility of metallic silver sputtering on tissue sections for  
52  
53 MS analysis and high resolution imaging mass spectrometry (IMS) of olefins by laser  
54  
55 desorption ionization (LDI).<sup>58</sup>  
56  
57  
58  
59  
60

Please insert Fig. 9 here

1  
2  
3  
4  
5  
6 Fig. 9 presents MS/MS spectra and proposed fragmentation pathways for silver cationized  
7  
8 arachidonic acid, docosahexaenoic acid, cholesterol and triacylglyceride 52:3, acquired from a  
9  
10 kidney tissue section after silver deposition. The dry deposition of a nanometer scale silver  
11  
12 layer of  $16 \pm 2$  nm thickness was performed with a sputter coating system. This method could  
13  
14 be considered an interesting approach to increase the amount of information obtained from  
15  
16 tissue sections.<sup>58</sup>  
17  
18

19  
20 The group of Volmer presented recently an excellent paper on synthesis and  
21  
22 application of approx. 100 nm-thick layers of palladium and silver nanostructures prepared  
23  
24 with galvanic electrochemical deposition for application for SALDI MS of small biological  
25  
26 molecules. Authors tested new methods with fatty acids, triglycerides, carbohydrates, and  
27  
28 antibiotics. What is interesting is that the authors found that the potassium adducts were only  
29  
30 seen for nanostructure films of thickness lower than 100 nm, whereas Pd and Ag cluster ions  
31  
32 were primarily generated with films thickness of 120 nm and higher.<sup>48</sup> Although method  
33  
34 presented is well suited for detection of low molecular weight compounds, unfortunately, the  
35  
36 spectra presented in this work did not contain nanostructure-related peaks such as silver ion  
37  
38 peaks of formula  $\text{Ag}_x^+$  ( $x = 1, 2, 3\dots$ ) which could be used for precise internal calibration.  
39  
40  
41  
42

43  
44 Porous silver-nanoparticle-embedded thin films were recently produced by the sol-gel  
45  
46 method as described by Russell et al.<sup>59</sup> Films on glass surface were prepared by spin-coating  
47  
48 with complex solution containing tetraethyl orthosilicate, nitric acid, 2-ethoxyethanol and  
49  
50 silver nitrate. The freshly coated wafers were then thermally treated in air at 700 °C for over 7  
51  
52 h. Thin films were then taped directly to the surface of a standard stainless steel MALDI plate  
53  
54 with copper tape and used for analysis. Tested substances – angiotensin II and various  
55  
56 triglycerides and phosphatidylcholines were found on spectra in form of peaks of silver  
57  
58 adducts.<sup>59</sup>  
59  
60

1  
2  
3 Recently we presented a method of covering target plate with silver NPs before the  
4 analyte was applied to the target. A durable, nanoscale-thick layer of cationic silver  
5 nanoparticles is obtained of roughly 100 nm size, covering commercial and modified MALDI  
6 targets. The synthesis of AgNPs electrostatically bound to the steel target was conducted by  
7 reduction of silver trifluoroacetate with DHB in tetrahydrofuran (THF) at room temperature,  
8 directly over the steel target. Sample preparation for analysis required only placement of 0.5-2  
9  $\mu\text{L}$  of the sample solution and air-drying. Several groups of compounds of different polarity,  
10 such as amino acids, saccharides, nucleosides, glycosides, sulfonic acids, aldehydes and  
11 nucleic bases, were analyzed with this method. The cationic silver nanoparticles allowed  
12 detection of D-ribose at attomolar levels, as well as analysis of biological samples such as  
13 urine and blood serum.<sup>47,51</sup> Moreover, the first application of monoisotopic  $^{109}\text{Ag}$ NPs enabled  
14 higher sensitivity, mass accuracy, and resolution, due to simplification of isotopic patterns of  
15 both analyte and silver ions.<sup>60</sup>

16  
17  
18  
19  
20  
21  
22  
23  
24  
25  
26  
27  
28  
29  
30  
31  
32  
33  
34  
35  
36 Please insert Fig. 10 here  
37  
38  
39  
40

41 Presented results documented the monoisotopic methods, compared to those using natural Ag,  
42 to enable roughly 2-fold higher intensities for  $^{109}\text{Ag}^+$  ionized adducts (Fig. 10B), but even 10-  
43 to 100-fold higher for complex species used for calibration, such as  $^{109}\text{Ag}_5^+ - ^{109}\text{Ag}_{20}^+$  (Fig.  
44 10A). The spectrum of D-ribose on  $^{109}\text{Ag}$ NPET (Fig. 10C) shows the ribose peak to contain  
45 only one line assigned to  $[\text{ribose} + ^{109}\text{Ag}]^+$  ion at  $m/z$  256.962.<sup>56</sup> Similar methodology applying  
46 reduction of silver over solid surface by dihydroxyaromatic species was presented by Hong et  
47 al. Mentioned authors reduced silver ions with surface-bound polydopamine and tested this  
48 new nanostructures for ionization efficiency of small peptide.<sup>61</sup> Besides high ionization  
49  
50  
51  
52  
53  
54  
55  
56  
57  
58  
59  
60

1  
2  
3 efficiency towards peptides, spectra presented in this work contain visible chemical  
4 background peaks, probably due to the fact that surface consist of organic network.  
5  
6  
7  
8  
9

### 10 **AgNPs in LDI MS imaging**

11  
12 MALDI-imaging mass spectrometry (MALDI-IMS) is a two-dimensional MALDI-MS  
13 technique used to visualize the spatial distribution of biomolecules without extraction,  
14 purification, separation, or labeling of biological samples. One of the critical limitations of the  
15 spatial resolution of MALDI-IMS is the size of the organic matrix crystal and the analyte  
16 migration during the matrix application process. To overcome these problems, researchers  
17 tried to use nanoparticles as substitutes of organic matrices.<sup>58,62</sup> Chaurand's group that was  
18 mentioned earlier presented utility of silver sputtering for imaging of brain tissue. What is  
19 interesting, authors improved resolution by oversampling<sup>63</sup> of the laser minimum raster (i.e.,  
20 20  $\mu\text{m}$ ) using the smallest step size of the sample stage (5  $\mu\text{m}$ ). With this methodology  
21 applied, ion images for silver cationized cholesterol were obtained within the tissue such as  
22 the mouse brain cerebellar cortex, the granular region, and the cerebellar lobules.<sup>58</sup> It should  
23 be noted that full ablation at each pixel's position is necessary for described oversampling  
24 procedure to be valid.  
25  
26  
27  
28  
29  
30  
31  
32  
33  
34  
35  
36  
37  
38  
39  
40  
41  
42

43  
44 Lee group applied LDI MS imaging focused on silver ion adduct of membrane-bound  
45 cholesterol for detection of individual astrocytes. The cells were covered with silver  
46 nanostructures by spraying from a nebulizer eight times to ensure homogeneous sample  
47 coverage and inhibit aggregation of silver products during the evaporation of solvent. What is  
48 interesting, authors found out that cholesterol was almost an exclusive cellular component that  
49 was observed in MS spectra.<sup>64</sup>  
50  
51  
52  
53  
54  
55  
56

57  
58 Jackson et al.<sup>65</sup> used AgNPs matrix to map several classes of lipids in heart tissue, by  
59 implanting AgNPs directly into a tissue sample and analyzing in positive ion mode. For  
60

1  
2  
3 example, whole coronal rat brain section could be coated with silver nanoparticles of 0.5–15  
4  
5 nm size, generated from a metal disk by magnetron sputtering.  
6  
7  
8  
9

10 Please insert Fig. 11 here  
11  
12  
13  
14  
15  
16

17 Mass spectra were collected from two distinct regions of interests: an area in the major blood  
18 vessels region of the heart (Fig. 11C) and an area representing the myocardium (Fig. 11d).<sup>65</sup>  
19  
20 Of note is that triacylglycerols, essential energy storage lipids, were uneasy to identify with  
21 organic MALDI matrix (DHB), probably due to the presence of positively charged  
22 phosphatidylcholines. In contrast, AgNPs showed high selectivity of ionization of low  
23 polarity triacylglycerol (TAG) species, resulting in mass spectra of the vessels region of the  
24 heart, dominated by TAG peaks, and those of the myocardium region, containing higher  
25 abundance of phosphatidylcholine (PCs) and phosphatidylethanolamine (PEs) species.<sup>65</sup>  
26  
27  
28  
29  
30  
31  
32  
33  
34  
35

36 Recently, Ewing group has presented interesting application of silver and gold  
37 nanoparticles enabling the sample to be compatible with LDI and secondary ion mass  
38 spectrometry (SIMS) techniques. Application of Ag and Au nanoparticles to the lipid sample  
39 containing 1-palmitoyl-2-oleoyl-sn-glycero-3-phosphocholine (POPC) allowed POPC lipid  
40 fragments to be detected using LDI in both positive and negative polarities. Furthermore,  
41 authors observed two-fold SIMS signal yield enhancement for the  $m/z$  184 and 86 POPC  
42 fragments peaks as well as for the POPC protonated ion ( $m/z$  760).<sup>66</sup>  
43  
44  
45  
46  
47  
48  
49  
50  
51  
52

53 A new approach was developed for the visualization of fatty acids in mouse liver and  
54 retinal samples by using silver nanoparticles in nanoparticle-assisted laser  
55 desorption/ionization imaging mass spectrometry (nano-PALDI-IMS) in negative ion mode.  
56  
57  
58  
59  
60 The  $3.84 \pm 0.45$  nm AgNPs used were prepared from the precursors -  $n\text{-C}_{13}\text{H}_{27}\text{COOAg}$  and

1  
2  
3 stearylamine.<sup>15,62</sup> AgNPs modified with alkylcarboxylates and alkyl amines were used for  
4 nano-PALDI-IMS to identify fatty acids in mouse liver sections. Notably these fatty acids  
5  
6  
7 could not be detected using DHB matrix.  
8  
9

10  
11  
12 Please insert Fig. 12 here  
13  
14  
15

16  
17 Mass spectra are presented of three different amounts of palmitic acid (Fig. 12, a-c)  
18 and reconstructed ion images for  $m/z$  255.3 (Fig. 12f) corresponding to palmitic acid, with the  
19 S/N ratios of 70.3, 12.8, and 2.0 for palmitate quantities of 500 pmol, 50 pmol and 5 pmol,  
20 respectively. Apparently this imaging system allowed the palmitic acid detection limit as low  
21 as 50 pmol.<sup>62</sup>  
22  
23  
24  
25  
26  
27  
28  
29

30  
31  
32 Please insert Fig. 13 here  
33  
34  
35

36 Silver nanoparticles were also employed to map the distribution of fatty acids in mouse retinal  
37 sections, with detected ion images corresponding to seven classes of fatty acids.<sup>62</sup>  
38  
39

40  
41 A series of interesting improvements of LDI MS ion trap imaging system was  
42 presented by Lee group. Mentioned group managed to change typical laser light optical  
43 system to optical fiber with 25  $\mu\text{m}$  core diameter resulting in  $\sim 12$   $\mu\text{m}$  spatial resolution  
44 allowing MS visualization at single cell level.<sup>62</sup> Plant flower and root compounds were  
45 ionized with assistance of colloidal silver sprayed over biological material with the use of  
46 custom made oscillating capillary nebulizer. Application of mentioned improvements resulted  
47 in analysis of *Arabidopsis thaliana* flower material focused on long-chain compounds such as  
48 alkanes, alcohols, fatty acids and ketones containing 27-31 carbon atoms.  
49  
50  
51  
52  
53  
54  
55  
56  
57  
58  
59  
60

1  
2  
3 The method of covering of standard MALDI target with monoisotopic cationic  $^{109}\text{Ag}$   
4 nanoparticles ( $^{109}\text{AgNPs}$ ) was demonstrated to be useful for high-resolution mass  
5 spectrometry imaging of organic and inorganic compounds, of endo- and exogenous origin,  
6 present on a fingerprint.<sup>51</sup> The fingerprint was easily transferable to the modified plate, using  
7 vinyl duct tape.  $^{109}\text{AgNPET}$  could be also used to perform mass spectrometry imaging  
8 visualization of foreign substance placed on a fingertip (e.g. Fig. 14).<sup>68</sup> Fingermarks were  
9 recently also imaged by Lauzon et al. with the use of sputtered silver.<sup>69</sup>  
10  
11  
12  
13  
14  
15  
16  
17  
18  
19  
20  
21

22 Please insert Fig. 14 here  
23  
24  
25  
26  
27  
28  
29  
30

### 31 **Conclusions**

32  
33  
34 Recent LDI MS applications for detecting chemical compounds with aid of silver  
35 nanostructures are reviewed. A laser desorption/ionization systems has been successfully used  
36 to analyze the chemical composition of various compounds both ionic and nonionic, of low  
37 and high molecular weights. Methods presented in this work allow analysis of complex  
38 biological mixtures, such as blood plasma and urine, up to trace quantities of compounds.  
39 Many applications of silver nanostructures in LDI MS imaging are also discussed.  
40  
41 Localization of compounds in various types of plant and animal tissues, but also a possibility  
42 of forensic analysis of fingerprints with AgNP-supported LDI MS imaging, present a great  
43 potential for future development.  
44  
45  
46  
47  
48  
49  
50  
51  
52  
53  
54  
55  
56  
57  
58  
59  
60

## Acknowledgements

This work was supported by Bioorganic Chemistry Laboratory DS funding (Rzeszow University of Technology, Poland, 2015).

## References

- 1 M. Karas, D. Bachmann, U. Bahr, F. Hillenkamp, *Int. J. Mass Spectrom. Ion Process*, 1987, **78**, 53–68.
- 2 F. Hillenkamp, M. Karas, R.C. Beavis, B.T. Chait, *Anal. Chem.*, 1991, **63**, 1193A–1203A.
- 3 F. Hillenkamp, M. Karas, *Methods Enzymol.*, 1990, **193**, 280–295.
- 4 J. Albrethsen, *Clin. Chem.*, 2007, **53**, 852–858.
- 5 R. Knochenmuss, F. Dubois, M.J. Dale, R. Zenobi, *Rapid Commun. Mass Spectrom.*, 1996, **10**, 871–877.
- 6 M. Karas, F. Hillenkamp, *Anal. Chem.*, 1988, **60**, 2299–2301.
- 7 P.C. Lin, P.H. Chou, S.H. Chen, K.L. Liao, K.Y. Wang, Y.J. Chen, C.C. Lin, *Small*, 2006, **4**, 485–489.
- 8 B. Domon, R. Aebersold, *Science*, 2006, **312**, 212–217.
- 9 S. Berkenkamp, F. Kirpekav, F. Hillenkamp, *Science*, 1998, **281**, 260–262.
- 10 K.C. Ho, P.J. Tsai, Y.S. Lin, Y.C. Chen, *Anal. Chem.*, 2004, **76**, 7162–7168.
- 11 K. Shrivvas, H.F. Wu, *Rapid Commun. Mass Spectrom.*, 2007, **21**, 3103–3108.
- 12 K. Shrivvas, H.F. Wu, *J. Mass Spectrom.*, 2007, **42**, 1637–1644.
- 13 R. Pilolli, F. Palmisano, N. Cioffi, *Anal. Bioanal. Chem.*, 2012, **402**, 601–623.
- 14 K. Tanaka, H. Waki, Y. Ido, S. Akita, Y. Yoshida, T. Yoshida, *Rapid Commun. Mass Spectrom.*, 1988, **2**, 151–153.

- 1  
2  
3 15 N. Cioffi, L. Colaianni, R. Pilolli, C.D. Calvano, F. Palmisano, P.G. Zambonin, *Anal.*  
4  
5 *Bioanal. Chem.*, 2009, **394**, 1375-1383.  
6  
7  
8 16 J. Sunner, E. Dratz, Y.C. Chen, *Anal. Chem.*, 1995, **67**, 4335–4342.  
9  
10 17 M.J. Dale, R. Knochenmuss, R. Zenobi, *Anal. Chem.*, 1996, **68**, 3321–3332.  
11  
12 18 M. Schurenberg, K. Dreisewerd, F. Hillenkamp, *Anal. Chem.*, 1999, **71**, 221–229.  
13  
14 19 Y.E. Silina, M. Koch and D.A. Volmer, *J. Mass Spectrom.*, 2014, **49**, 468–480.  
15  
16 20 I.D.G. Macdonald, W.E. Smith, *Langmuir*, 1999, **12**, 706–713.  
17  
18 21 L. Hua, J. Chen, L. Ge, S.N. Tan, *J. Nanopart. Res.*, 2007, **9**, 1133-1138.  
19  
20 22 S.D. Sherrod, A.J. Diaz, W.K. Russell, P.S. Cremer, D.H. Russell, *Anal. Chem.*, 2008, **80**,  
21  
22 6796-6799.  
23  
24  
25 23 K. Shrivasa, H.F. Wu, *Rapid Commun. Mass Spectrom.*, 2008, **22**, 2863–2872.  
26  
27  
28 24 F. Frederix, J. Friedt, K. Choi, W. Laureyn, A. Campitelli, D. Mondelaers, G. Maes, G.  
29  
30 Borghs, *Anal. Chem.*, 2003, **75**, 6894–6900.  
31  
32  
33 25 C.L. Su, W.L. Tseng, *Anal. Chem.*, 2007, **79**, 1626-1633.  
34  
35  
36 26 C.H. Teng, K.C. Ho, Y.S. Lin, Y.C. Chen, *Anal. Chem.*, 2004, **76**, 4337-4342.  
37  
38  
39 27 P.R. Sudhir, H.F. Wu, Z.C. Zhou, *Anal. Chem.*, 2005, **77**, 7380-7385.  
40  
41  
42 28 K. Shrivasa, H.F. Wu, *Anal. Chem.*, 2008, **80**, 2583-2589.  
43  
44  
45 29 P.T. Sudhir, K. Shrivasa, Z.C. Zhou, H.F. Wu, *Rapid Commun. Mass Spectrom.*, 2008, **22**,  
46  
47 3076–3086.  
48  
49  
50 30 S.K. Kailasaa, H.F. Wu, *Talanta*, 2010, **83**, 527–534.  
51  
52  
53 31 L. Shastri, H. N. Abdelhamid, M. Nawaz, H.-F. Wu, *RSC Adv.*, 2015, **5**, 41595-41603.  
54  
55  
56 32 M. Inuta, R. Arakawa, H. Kawasaki, *Anal. Methods*, 2013, **19**, 5031-5036.  
57  
58  
59 33 M. Yang, T. Fujino, *Chem. Phys. Lett.*, 2013, **576**, 61–64.  
60  
61 34 T.C. Chiu, L.C. Chang, C.K. Chiang, H.T. Chang, *J. Am. Soc. Mass Spectrom.*, 2008, **19**,  
1343–1346.

- 1  
2  
3 35 P.C. Lee, D. Meisel, *J. Phys. Chem.*, 1982, **86**, 3391–3395.  
4  
5  
6 36 M.T. Wang, M.H. Liu, C.R.C. Wang, S.Y. Chang, *J. Am. Soc. Mass Spectrom.*, 2009, **20**,  
7  
8 1925–1932.  
9  
10 37 Y. Gholipour, S.L. Giudicessi, H. Nonami, R. Erra-Balsells, *Anal. Chem.*, 2010, **82**, 5518–  
11  
12 5526.  
13  
14  
15 38 B. Nie, R.N. Masyukoa, P.W. Bohn, *Analyst*, 2012, **137**, 1421-1427.  
16  
17  
18 39 B. Vrbkova, V. Roblová, E.S. Yeung, J. Preisler, *Journal of Chromatography A*, 2014, **1358**,  
19  
20 102-109.  
21  
22 40 S. Taira, H. Taguchi, R. Fukuda, K. Uematsu, Y. Ichiyanagi, Y. Tanaka, Y. Fujii, and H.  
23  
24 Katano, *Mass Spectrometry*, 2014, **3**, S0025/1-S0025/5  
25  
26  
27 41 T.C. Chiu, *Int. J. Mol. Sci.*, 2014, **15**, 7266-7280.  
28  
29  
30 42 J.J. Bright, M.A. Claydon, M. Soufian, D.B. Gordon, *J. Microbiol. Methods*, 2002, **48**, 127–  
31  
32 138.  
33  
34 43 Z.P. Yao, P.A. Demirev, C. Fenselau, *Anal. Chem.*, 2002, **74**, 2529–2534.  
35  
36 44 C.H. Lee, J. Gopal, H.F. Wu, *Biosensors and Bioelectronics*, 2012, **31**, 77– 83.  
37  
38 45 J. Gopal, H.-F. Wu, C.H. Lee, *Analyst*, 2011, **136**, 5077-5083.  
39  
40  
41 46 J. Gopal, M. Manikandan, N. Hasan, C.-H. Lee, H.-F. Wu, *J. Mass Spectrom.*, 2013, **48**, 119–  
42  
43 127.  
44  
45  
46 47 J. Nizioł, Z. Zieliński, W. Rode, T. Ruman, *Int. J. Mass Spectrom.*, 2013, **335**, 22-32.  
47  
48 48 Y.E. Silina, F. Meier, V.A. Nebolsin, M. Koch, D.A. Volmer, *J. Am. Soc. Mass Spectrom.*,  
49  
50 2014, **25**, 841-851.  
51  
52  
53 49 M.F. Wyatt, S. Ding, B.K. Stein, A.G. Brenton, R.H. Daniels, *J. Am. Soc. Mass Spectrom.*,  
54  
55 2010, **21**, 1256–1259.  
56  
57  
58 50 K.P. Law, J.R. Larkin, *Bioanal. Chem.*, 2011, **399**, 2597-622.  
59  
60 51 J. Nizioł, W. Rode, B. Laskowska, T. Ruman, *Anal. Chem.*, 2013, **85**, 1926-1931.

- 1  
2  
3 52 C. Lei, K. Qian, O. Noonan, A. Nouwens, C. Yu, *Nanoscale*, 2013, **5**, 12033-12042.  
4  
5  
6 53 C.-C. Hu, M.-F. Huang, H.-T. Chang, *Bioanalysis*, 2013, **5**, 633-635.  
7  
8 54 J. A. Stolee, B. N. Walker, V. Zorba, R. E. Russo, A. Vertes, *Phys. Chem. Chem. Phys.*, 2012,  
9  
10 **14**, 8453-8471.  
11  
12 55 J. Wei, J.M. Buriak, G. Siuzdak, *Nature*, 1999, **399**, 243–246.  
13  
14  
15 56 O.A. Boryak, M.V. Kosevich, V.V. Chagovets, V.G. Zobnina, V.V. Orlov, V.S. Shelkovsky,  
16  
17 S.G. Stepanian, *J. Anal. Chem.*, 2012, **67**, 994–1000.  
18  
19  
20 57 H. Yan, N. Xua, W.-Y. Huang, H.-M. Hana, S.-J. Xiaoa, *International Journal of Mass*  
21  
22 *Spectrometry*, 2009, **281**, 1-7.  
23  
24  
25 58 M. Dufresne, A. Thomas, J. Breault-Turcot, J.-F. Masson, P. Chaurand, *Anal. Chem.*, 2013,  
26  
27 **85**, 3318–3324.  
28  
29  
30 59 R.C. Gamez, E.T. Castellana, and D.H. Russell, *Langmuir*, 2013, **29**, 6502-6507.  
31  
32  
33 60 J. Nizioł and T. Ruman, *Int. J. Chem. Eng. Appl.*, 2013, **2**, 46-49.  
34  
35  
36 61 S. Hong, J.S. Lee, J. Ryu, S.H. Lee, D.Y. Lee, D.-P. Kim, C. B. Park and H. Lee,  
37  
38 *Nanotechnology*, 2011, **22**, 494020/1-494020/7.  
39  
40  
41 62 T. Hayasaka, N. Goto-Inoue, N. Zaima, K. Shrivasa, Y. Kashiwagi, M. Yamamoto, M.  
42  
43 Nakamoto, M. Setou, *J. Am. Soc. Mass Spectrom.*, 2010, **21**, 1446–1454.  
44  
45  
46 63 J. C. Jurchen, S. S. Rubakhin, J. V. Sweedler, *Journal of The American Society for Mass*  
47  
48 *Spectrometry*, 2005, **16**, 1654–1659.  
49  
50  
51 64 D.C. Perdian, S. Cha, J. Oh, D.S. Sakaguchi, E.S. Yeung and Y.J. Lee., *Rapid Commun. Mass*  
52  
53 *Spectrom.*, 2010, **24**, 1147-1154.  
54  
55  
56 65 S.N. Jackson, K. Baldwin, L. Muller, V.M. Womack, J.A. Schultz, C. Balaban, A.S. Woods,  
57  
58 *Anal. Bioanal. Chem.*, 2014, **406**, 1377-1386.  
59  
60  
61 66 A.S. Mohammadi, J.S. Fletcher, P. Malmberg and A.G. Ewing, *Surface and Interface*  
*Analysis*, 2014, **46(S1)**, 379-382.

1  
2  
3 67 J.H. Jun, et al., *Anal. Chem.*, 2010, **82**, 3255-3265.  
4

5 68 J. Nizioł, T. Ruman, *Anal. Chem.*, 2013, **85**, 12070–12076.  
6

7 69 N. Lauzon, M. Dufresne, V. Chauhan, P. Chaurand, *Journal of The American Society for*  
8

9 *Mass Spectrometry*, 2015, **26**, 878-886.  
10  
11  
12  
13  
14  
15  
16  
17  
18  
19  
20  
21  
22  
23  
24  
25  
26  
27  
28  
29  
30  
31  
32  
33  
34  
35  
36  
37  
38  
39  
40  
41  
42  
43  
44  
45  
46  
47  
48  
49  
50  
51  
52  
53  
54  
55  
56  
57  
58  
59  
60

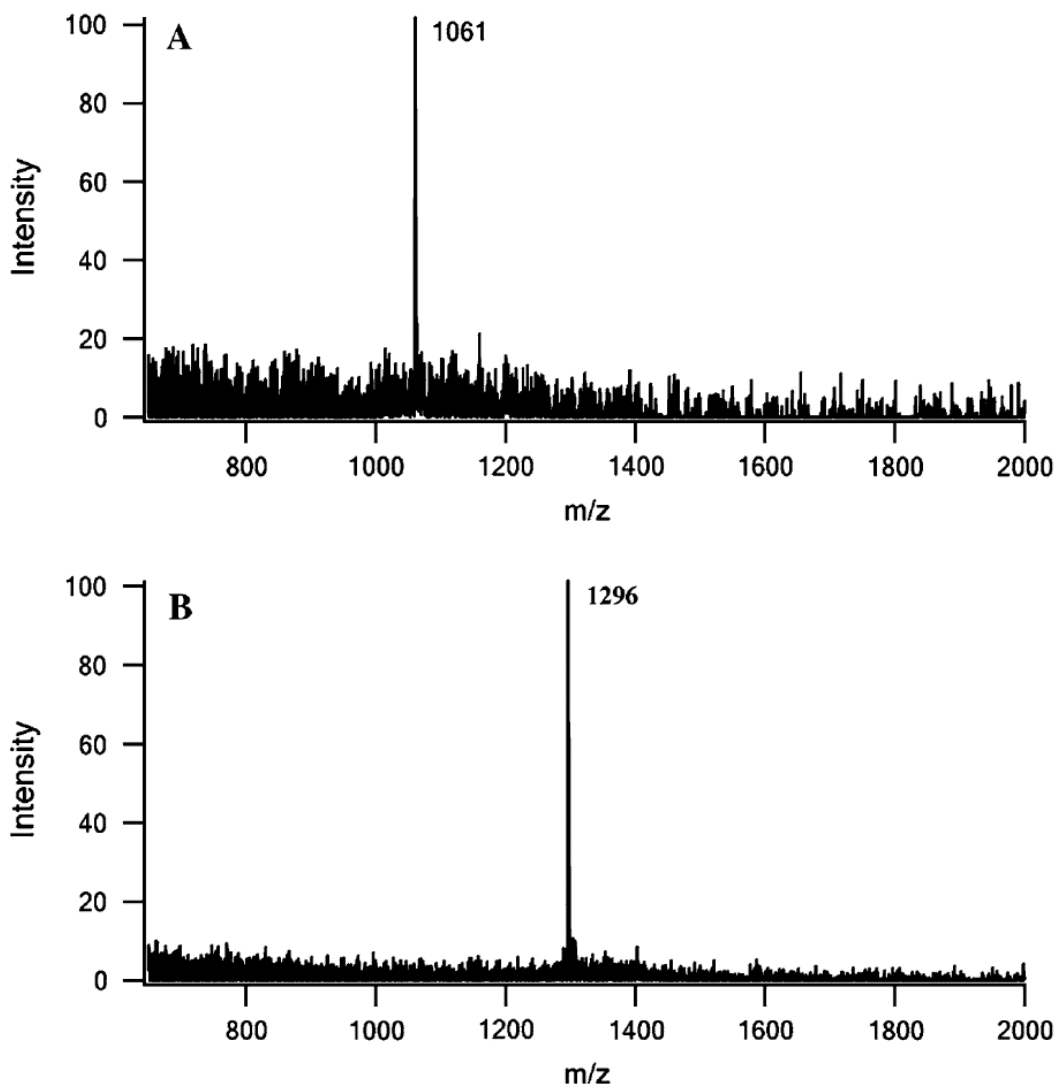


**Fig. 1** Nano-PALDI mass spectra of (A) bradykinin and (B) angiotensin I obtained with silver nanoparticles. Reprinted with permission from ref. 21.

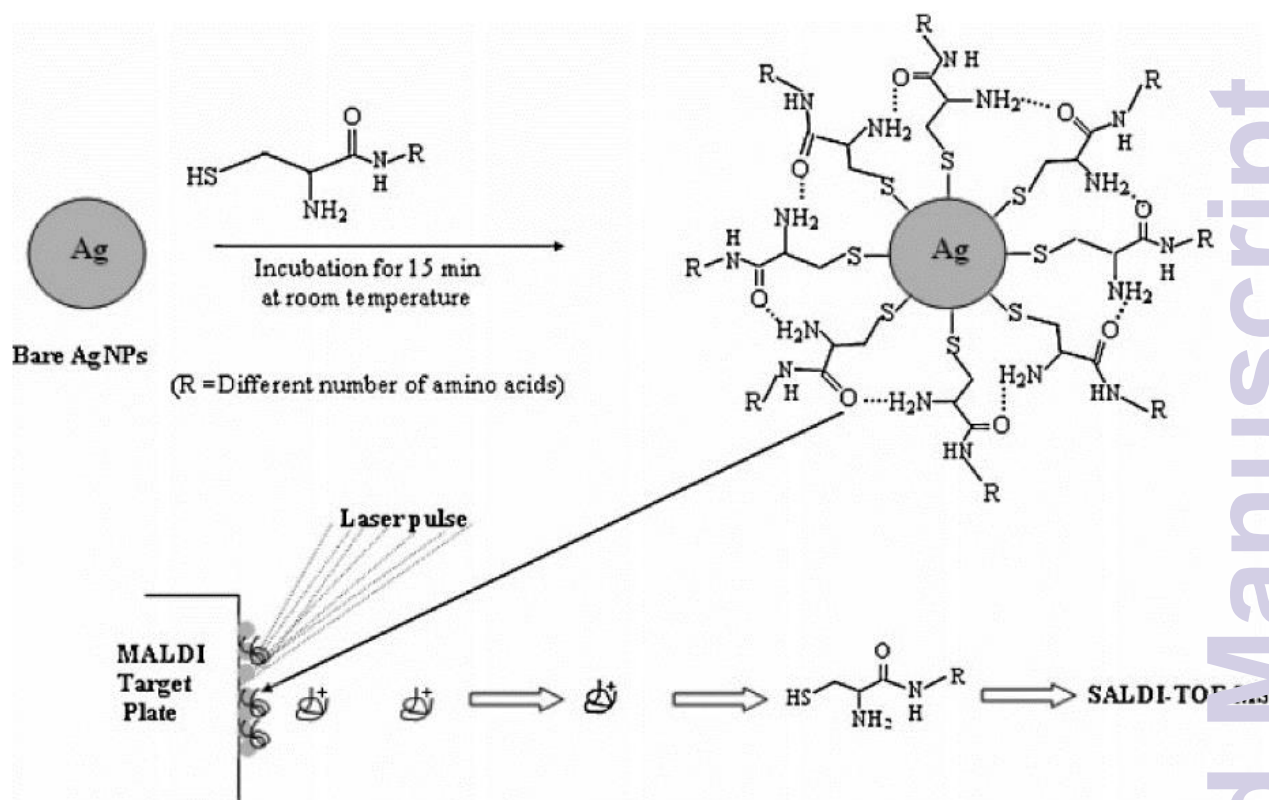


**Fig. 2** Reaction of AgNPs with thiols (upper part) and flow-chart of SALDI-ToF MS analysis with the use of AgNPs as preconcentration and ionization medium (lower part). Reprinted with permission from ref. 23.

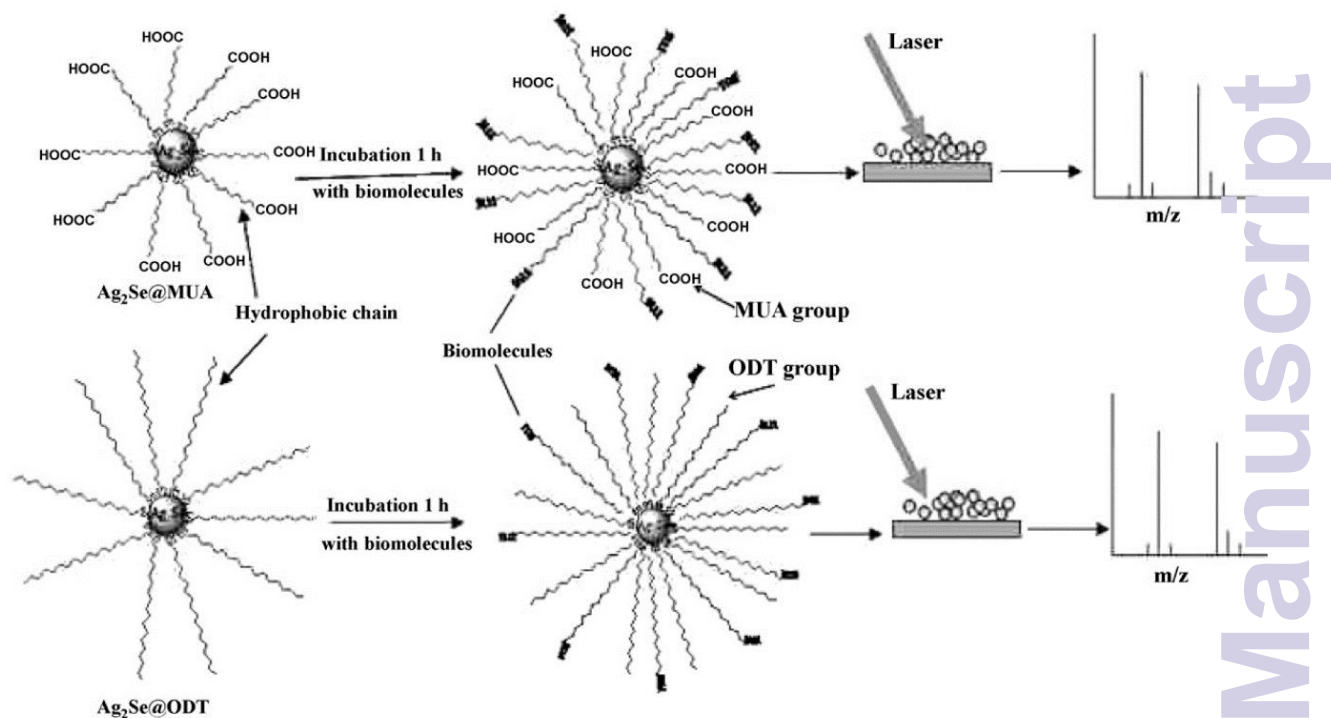


**Fig. 3** Schematic procedure for liquid-phase microextraction of hydrophobic peptides/proteins for nano-PALDI MS analysis with functionalized Ag<sub>2</sub>Se NPs. Reprinted with permission from ref. 30.

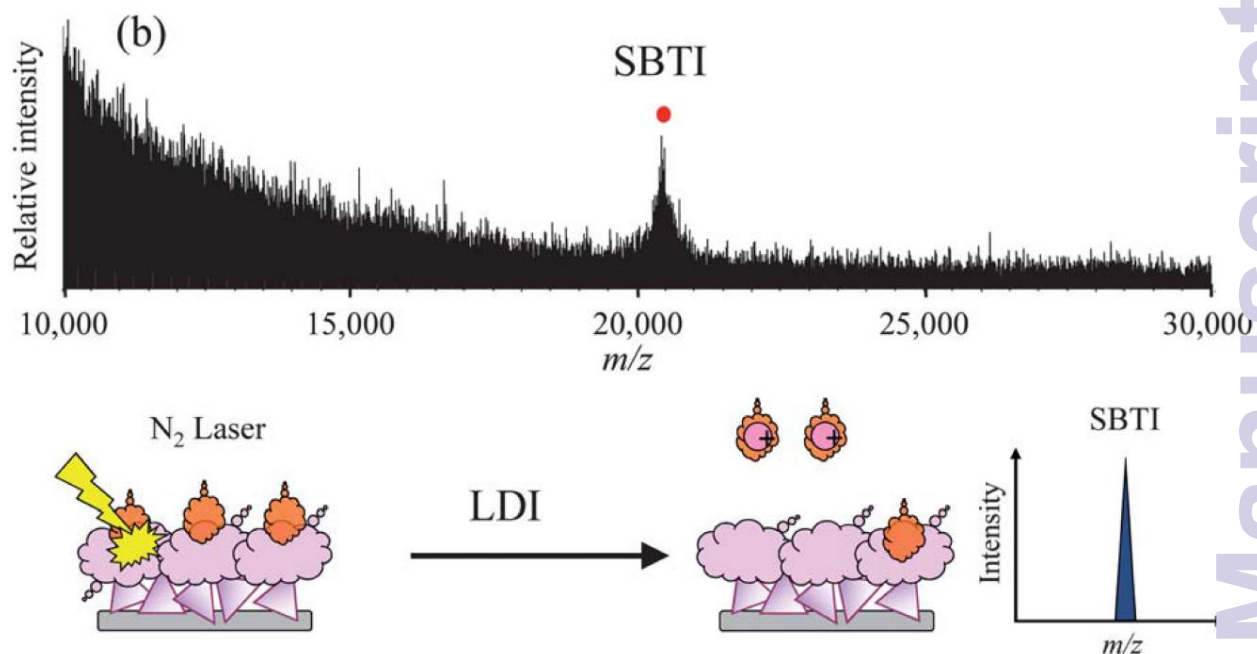


**Fig. 4** MALDI mass spectrum of SBTI (soybean trypsin inhibitor) obtained with the use of Trp-AgNPL system. Reprinted with permission from ref. 32.

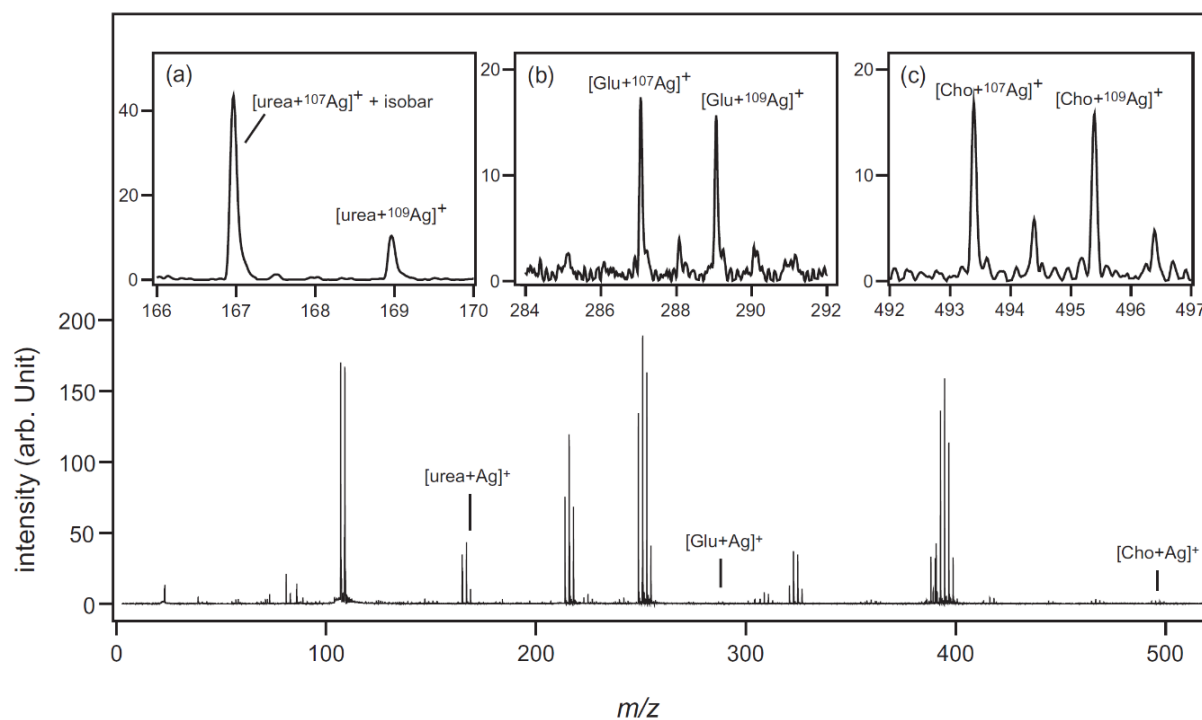


**Fig. 5** MS spectrum of human serum sample on AgNPs-NH<sub>4</sub>ZSM<sub>5</sub>. Regions containing peaks of urea (a), glucose (Glu, b) and cholesterol (Cho, c) are enlarged in the upper part of the figure. Reprinted with permission from ref. 33.

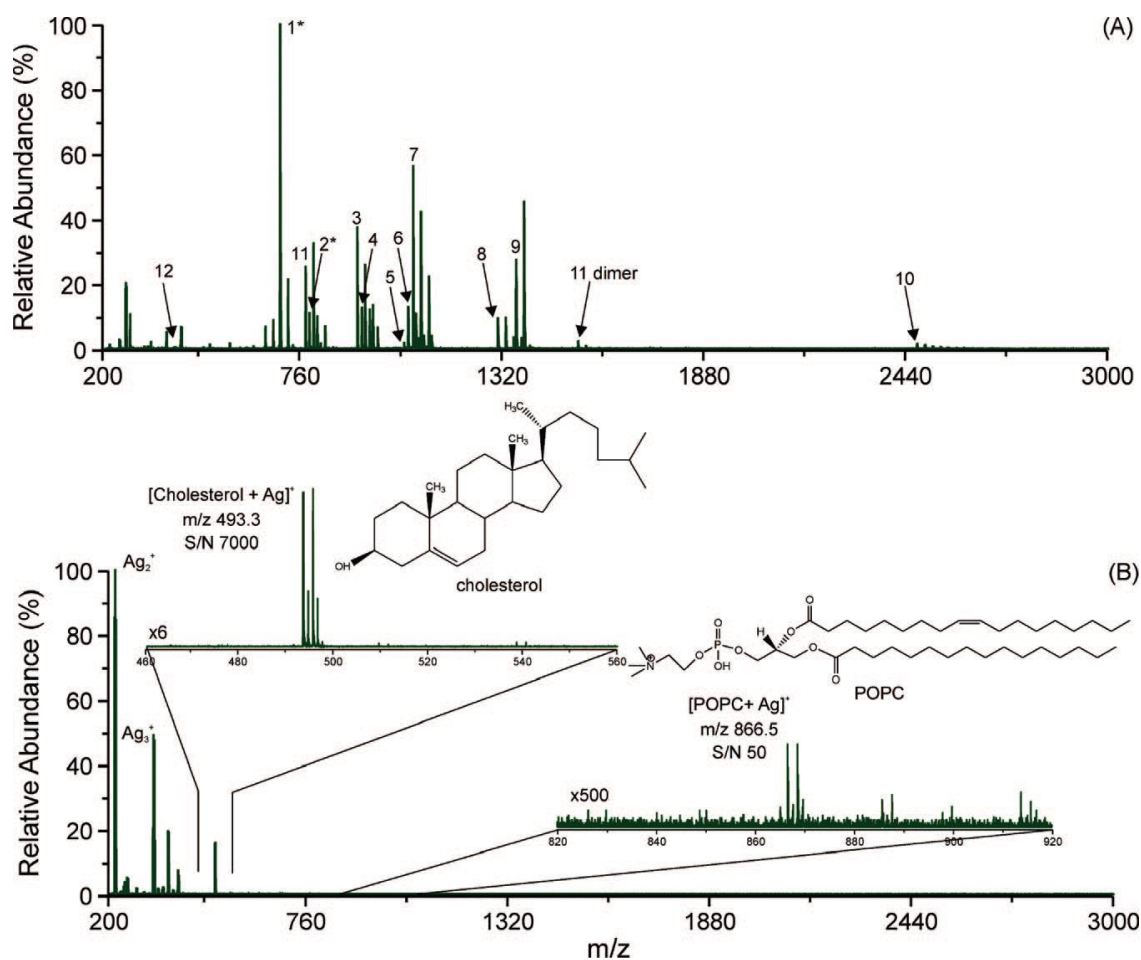


**Fig. 6** MS spectra of peptide/phosphocholine/cholesterol mixture obtained with DHB/AgNO<sub>3</sub> (A) and AgNPs (B). Reprinted with permission from ref. 22.

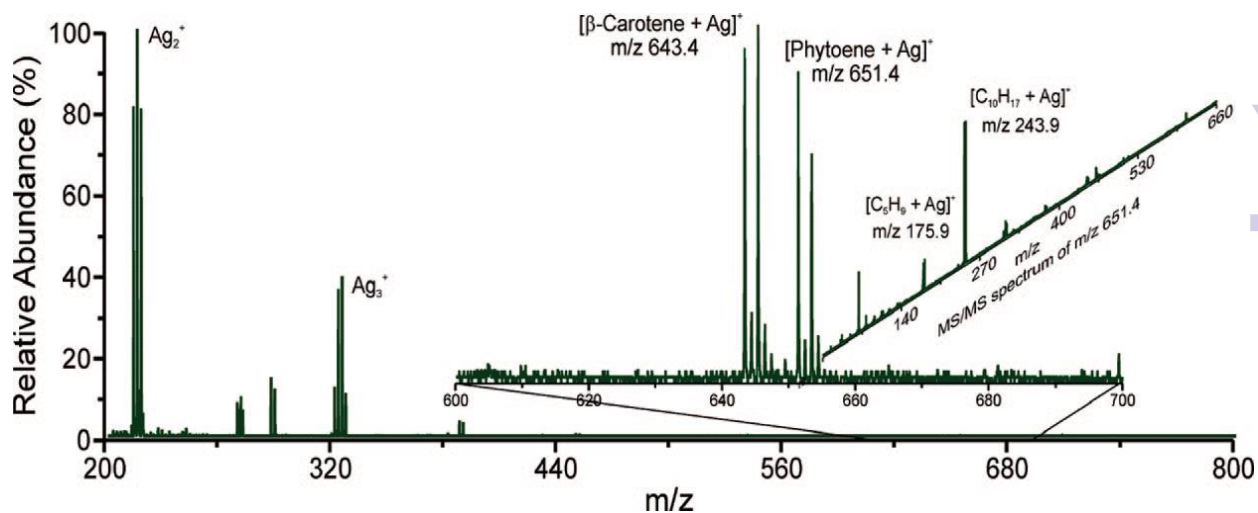


**Fig. 7** Mass spectrum of freshly squeezed carrot juice obtained with 20 nm AgNPs. The inset presents tandem MS fragmentation spectrum for the phytoene ion. Reprinted with permission from ref. 22.

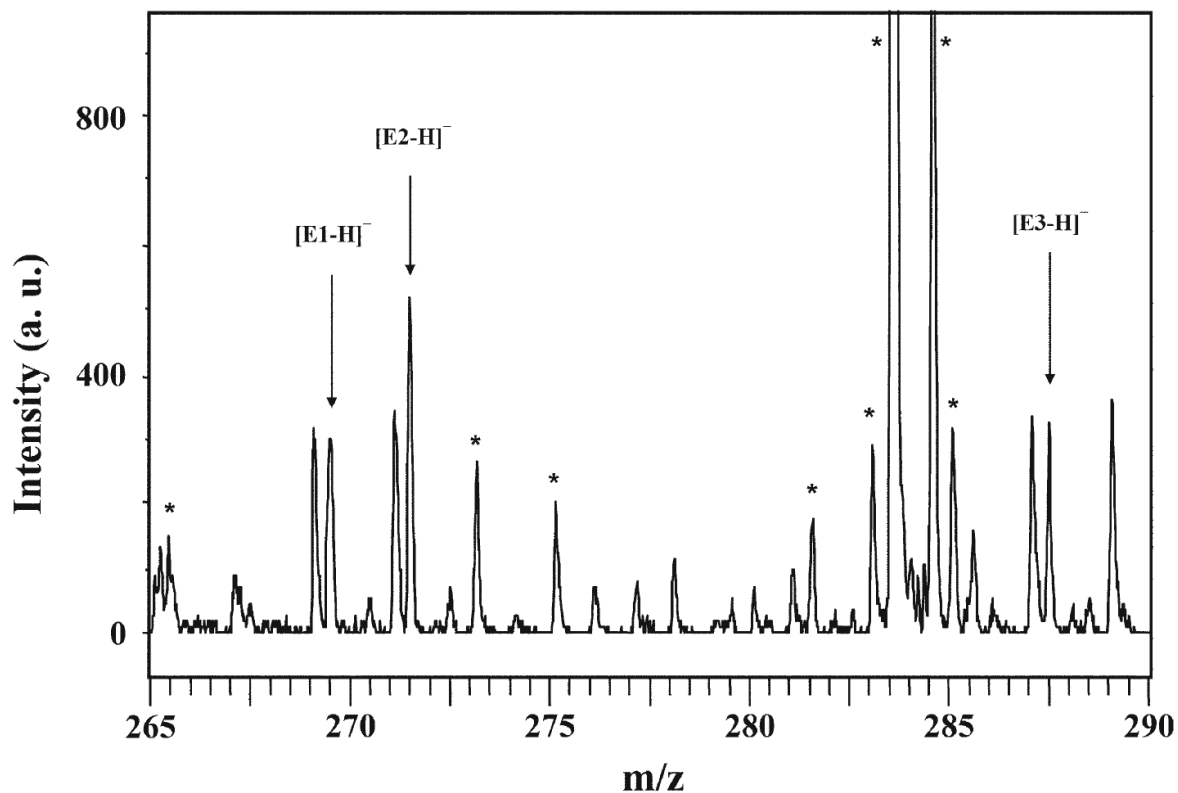


**Fig. 8** SALDI mass spectrum in negative ion mode of a mixture of E1 (100  $\mu$ M), E2 (10  $\mu$ M), and E3 (100  $\mu$ M) estrogens. Peaks of the chemical background are marked by asterisks.

Reprinted with permission from ref. 34.

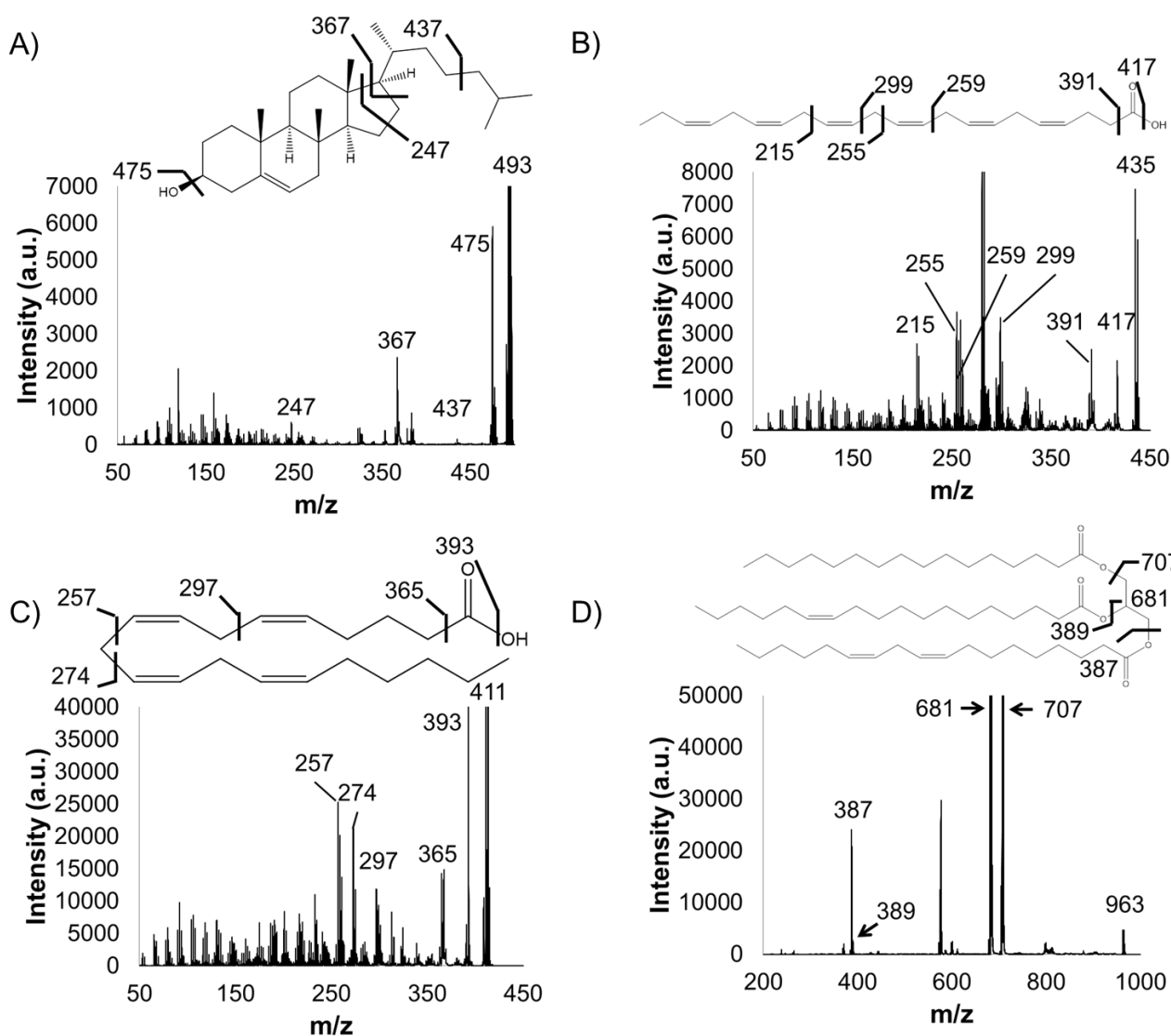


**Fig. 9** MS/MS spectra of cholesterol (A), docosahexaenoic acid (B), arachidonic acid (C), and triacylglyceride 52:3 (D) acquired from a kidney tissue section after silver sputtering with fragmentation pathways proposed for each molecule. Reprinted with permission from ref. 58.

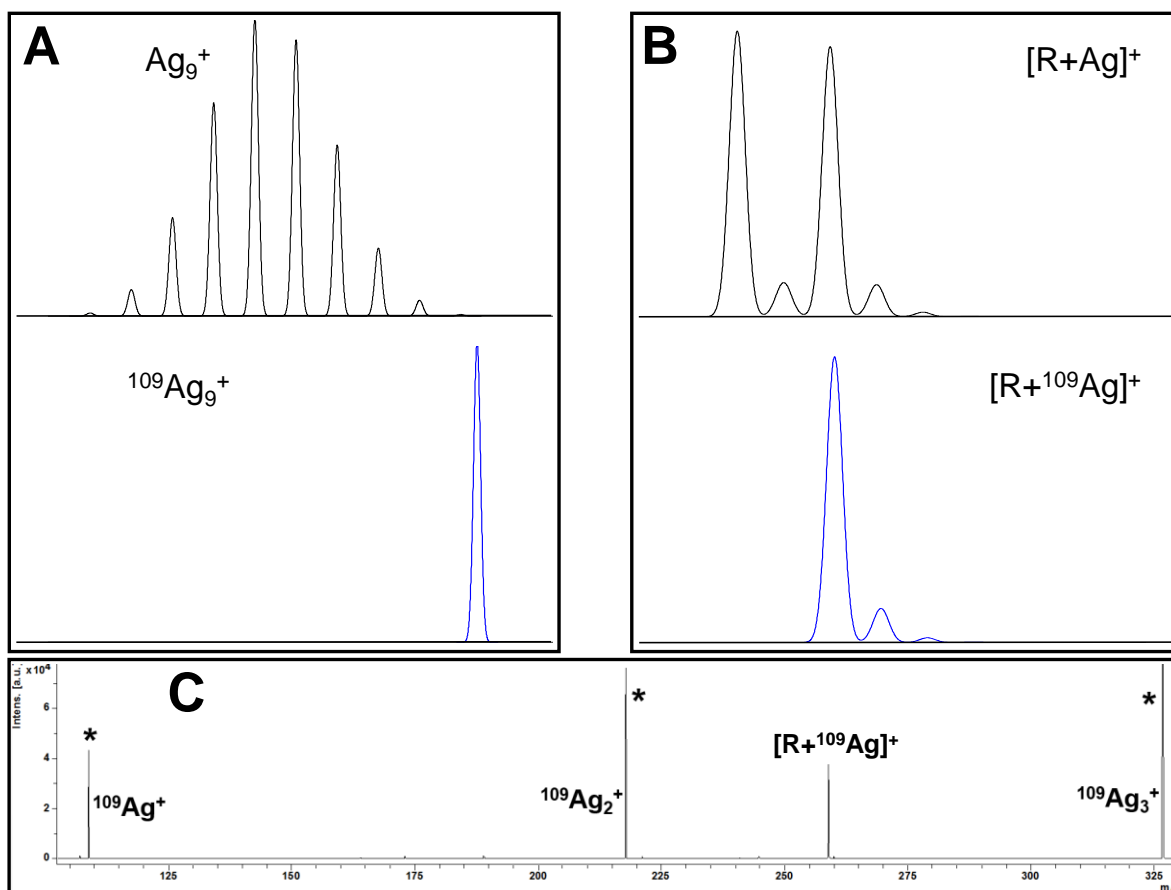


**Fig. 10** Calculated isotopic distributions of a  $^{109}\text{Ag}_9^+$  (A, bottom),  $\text{Ag}_9^+$  (A, top),  $[\text{ribose}+^{109}\text{Ag}]^+$  (B, bottom) and  $[\text{ribose}+\text{Ag}]^+$  (B, top) ions along with  $^{109}\text{AgNPET}$  mass spectrum (C) of D-ribose (R) in positive reflectron mode. Reprinted with permission from ref. 60.

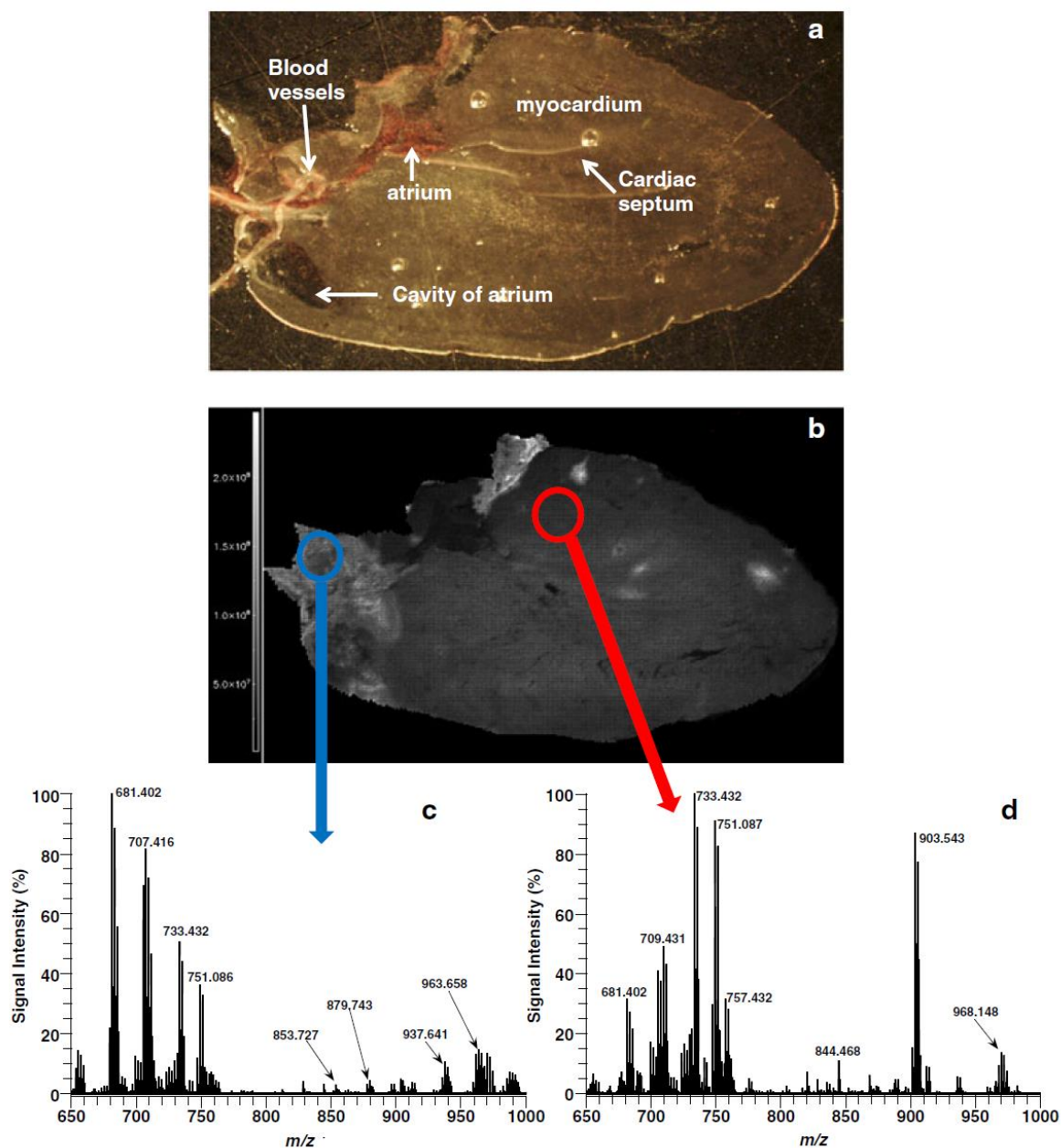


**Fig. 11** Optical microscope photograph of a heart section prior to AgNP implantation (a); MALDI image of the heart section with AgNPs in positive ion mode (b); average mass spectra of vessels region (c) and myocardium area (d). Reprinted with permission from ref. 65.

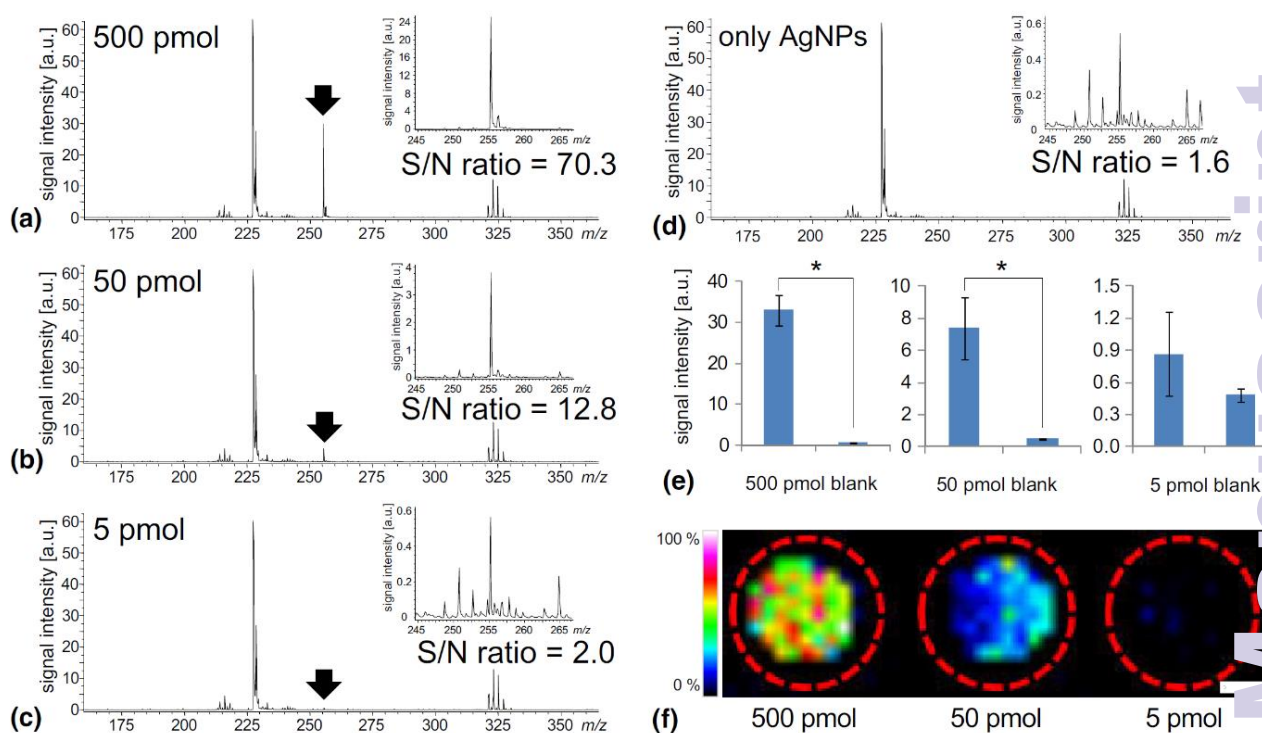


**Fig. 12** LOD determination of palmitic acid in nano-PALDI-IMS by analysis of S/N ratio (a-c) on the spots with different amounts of this acid (f). Reprinted with permission from ref. 62.

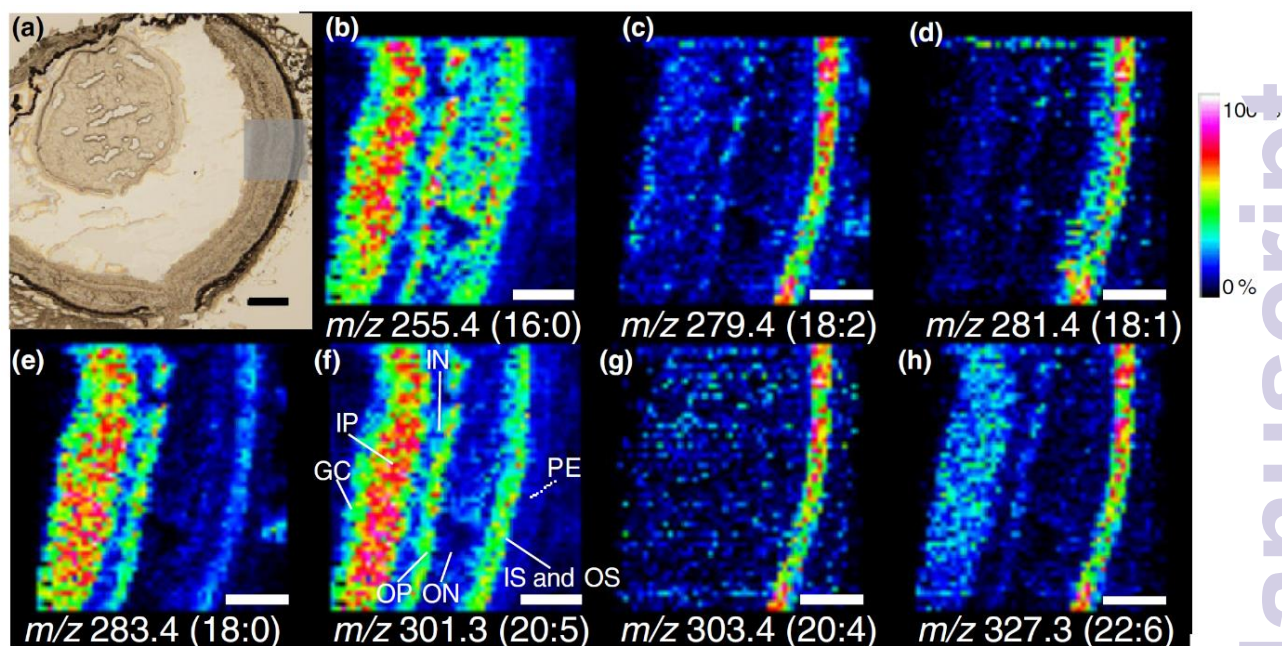


**Fig. 13** Identification of fatty acids in mouse retinal sections in nano-PALDI-IMS. The mouse retinal section was sliced to a thickness of 10  $\mu\text{m}$  (A). The ion images were reconstructed from the peaks corresponding to seven fatty acids (B-H). Reprinted with permission from ref. 62.

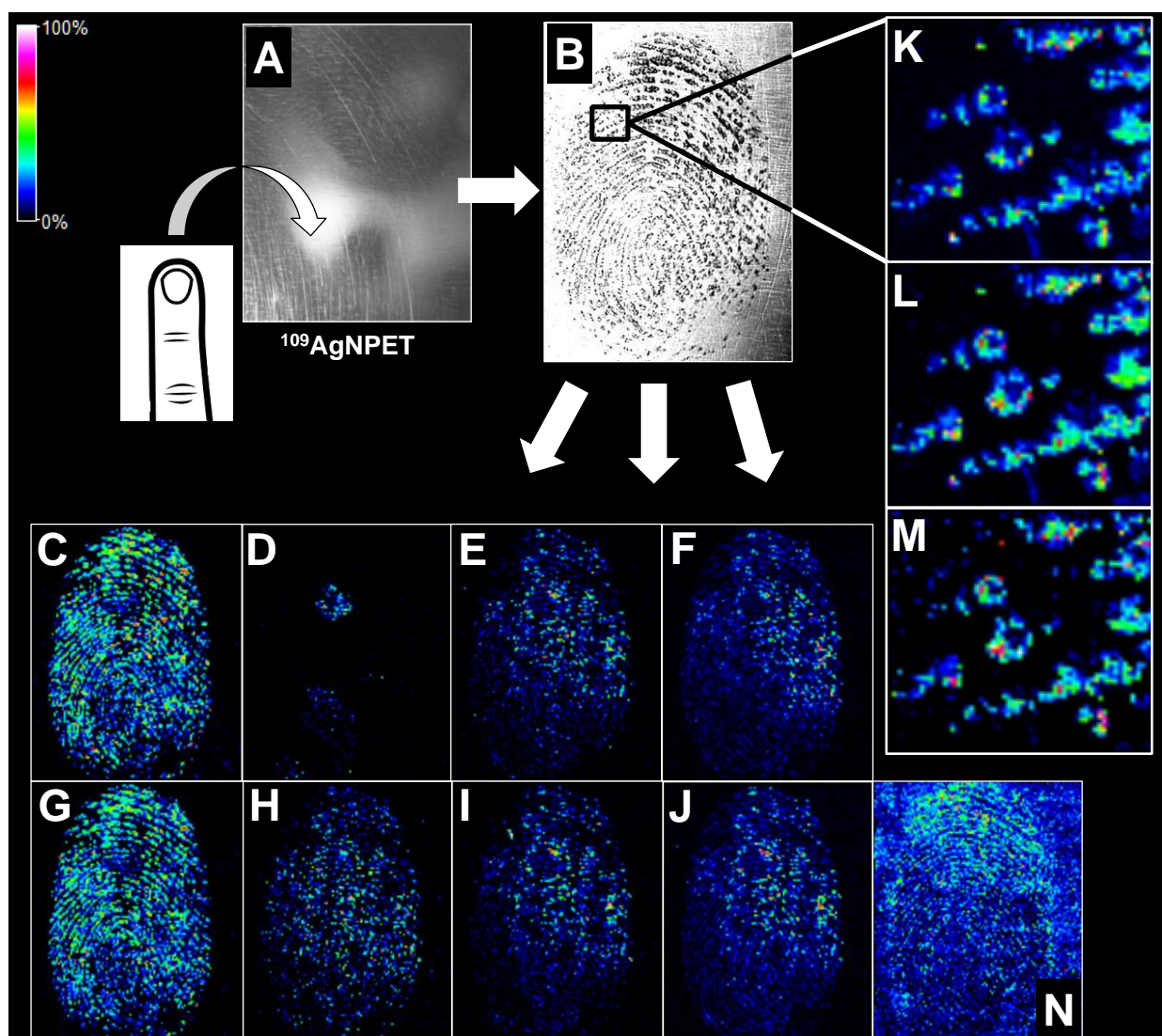


**Fig. 14** Latent fingerprint MSI analysis (150  $\mu\text{m}$  pixel size) on  $^{109}\text{AgNPET}$ . A, B – optical microscope images of a  $^{109}\text{AgNPET}$  surface without (A) and with a fingerprint (B). C-J – graphical representations (TIC normalization) of fingerprint compounds at  $m/z$ : 131.895 (C), 315.036 (D), 312.301 (E), 240.259 (F), 147.864 (G), 396.150 (H), 284.286 (I), 311.303 (J) and 168.982 (N). The K ( $m/z$  96.922), L ( $m/z$ 80.948) and M ( $m/z$ 83.022) representations are from another experiment of 50 x 50  $\mu\text{m}$ -spatial resolution. All representations are within  $\pm 0.02$   $m/z$ . Reprinted with permission from ref. 68.

1  
2  
3  
4  
5  
6  
7  
8  
9  
10  
11  
12  
13  
14  
15  
16  
17  
18  
19  
20  
21  
22  
23  
24  
25  
26  
27  
28  
29  
30  
31  
32  
33  
34  
35  
36  
37  
38  
39  
40  
41  
42  
43  
44  
45  
46  
47  
48  
49  
50  
51  
52  
53  
54  
55  
56  
57  
58  
59  
60

Analyst Accepted Manuscript